Journal of Volcanology and Geothermal Research 392 (2020) 106754

Contents lists available at ScienceDirect

Journal of Volcanology and Geothermal Research

journal homepage: www.elsevier.com/locate/jvolgeores

Alteration progress within the Surtsey hydrothermal system, SW Iceland – A time-lapse petrographic study of cores drilled in 1979 and 2017

Simon Prause [a,*], Tobias Björn Weisenberger [a], Piergiulio Cappelletti [b], Carla Grimaldi [b], Concetta Rispoli [b], Kristján Jónasson [c], Marie D. Jackson [d], Magnús Tumi Gudmundsson [e]

[a] Iceland GeoSurvey (ÍSOR), Reykjavík, Iceland
[b] Dipartimento di Scienze della Terra, dell'Ambiente e delle Risorse (DiSTAR), Università degli Studi di Napoli Federico II, Naples, Italy
[c] Icelandic Institute of Natural History (IINH), Garðabær, Iceland
[d] Department of Geology and Geophysics, University of Utah, Salt Lake City, USA
[e] Nordvulk, Institute of Earth Sciences, University of Iceland, Reykjavík, Iceland

ARTICLE INFO

Article history:
Received 29 August 2019
Received in revised form 6 November 2019
Accepted 12 December 2019
Available online 13 December 2019

Keywords:
Surtsey volcano
ICDP
SUSTAIN
Palagonitization
Basaltic glass
Hydrothermal alteration

ABSTRACT

The evolution of hydrothermal alteration in glassy and variably palagonitized tuff, erupted as tephra in 1963–1964 on Surtsey, an island built in the offshore extension of Iceland's southeast rift zone, is documented through a comparative petrographic study of samples from drill cores recovered in 1979 and 2017. Time-lapse alteration within the low-temperature meteoric to seawater dominated hydrothermal system of the volcano is characterized in terms of secondary mineral contents, alteration rates and alteration style with depth. Between 1979 and 2017 palagonitization and cementation by secondary minerals has progressed into previously poorly altered parts of the system, leading to increased consolidation of the basaltic tephra. Alteration rates range between 1.05 and 42.5 $\mu m \cdot yr^{-1}$ for palagonitization of glass and 0.4–8.33 $\mu m \cdot yr^{-1}$ for pseudomorphic olivine replacement by clay minerals over a temperature interval of 47–140 °C. Five distinct zones of alteration style, distinguished through alteration mineralogy, development of authigenic phases over time, as well as degree of alteration are described. Alteration of basaltic tephra at Surtsey volcano is defined by an early stage of phillipsite and clay mineral formation, followed by a later stage of analcime and tobermorite formation as well as replacement of phillipsite below the water table in zone 2 between 65.4 and 138.4 m. Only minor advancement of alteration is detected in zone 3 between 138.4 and 150.3 m depth, where the primary tephra remains largely unpalagonitized and unconsolidated. In contrast, from 1979 to 2017 alteration has increased between 150.3 and 177.8 m depth, in zone 4, leading to rapid and extensive glass and olivine alteration. The quantification of these time-lapse hydrothermal alteration processes at Surtsey provides an important reference for studies of the evolution of young oceanic islands hosting hydrothermal systems.

1. Introduction

In active geothermal systems, hydrothermal fluid flow is known to cause changes in host rock mineral content via fluid-rock interaction, through processes such as geochemical leaching, as well as precipitation of secondary mineral phases from the equilibrating geothermal fluid. The formation of secondary minerals is essentially dependent on time, temperature, pressure, initial rock composition, dissolved aqueous species, pH, fluid-rock-ratio and porosity/permeability (Browne, 1978; Giggenbach, 1984; Henley et al., 1985; Pauly et al., 2011). Thus, the nature and quantitative composition of a hydrothermal system's secondary mineral assemblage at depth may be considered to be indicative of the physicochemical properties and history of both host rock and hydrothermal fluid (e.g. Weisenberger and Selbekk, 2009; Kousehlar et al., 2012; Spürgin et al., 2019). As the geothermal system undergoes change with time, these properties too will be subject to variation, thereby resulting in an altered chemistry of the hydrothermal fluid, as well as a shift in the stability of secondary minerals. The effects of time as well as chemical and thermal changes are therefore an important aspect to consider in the petrographic study of hydrothermal alteration.

Within systems containing fresh basaltic glass (sideromelane), heat and chemical interaction with circulating fluids may cause devitrification of the glass (Marshall, 1961; Crovisier et al., 2003), leading to the formation of a metastable alteration product called palagonite.

* Corresponding author.
E-mail addresses: simon.prause@isor.is (S. Prause), tbw@isor.is (T.B. Weisenberger).

https://doi.org/10.1016/j.jvolgeores.2019.106754
0377-0273/

Palagonite, first described by Von Waltershausen (1845), occurs as a yellow to dark reddish brown amorphous to cryptocrystalline gel-like phase, commonly found as a surface alteration product of sideromelane, which can fully replace the original basaltic glass at advanced stages of the reaction. Palagonitization is recognized as a key factor in the lithification of loose vitric basalt tephra, fortifying volcanic edifices against erosion and increasing slope stability (Schiffman et al., 2006; Frolova, 2010; Romagnoli and Jakobsson, 2015), as well as being of global importance for oceanic crust-seawater chemical budgets (Staudigel and Hart, 1983; Walton et al., 2005; Pauly et al., 2011; Gernon et al., 2016). Additionally, the formation of palagonite and associated authigenic mineral assemblages from sideromelane is widely considered as a natural counterpart to alteration processes that may take place in radioactive waste storage borosilicate glasses, making the study of basaltic glass alteration relevant for the assessment of challenges involved in the long-term storage of these hazardous materials (Techer et al., 2001; Crovisier et al., 2003; Parruzot et al., 2015). Despite this potential relevance, the mineralogical nature of palagonite and its formation mechanism remain subject of research. Generally, it is accepted today, that palagonite forms as a result of dissolution of sideromelane in conjunction with glass hydration, which is usually accompanied by the precipitation of diverse mineral assemblages (Stroncik and Schmincke, 2002; Crovisier et al., 2003; Drief and Schiffman, 2004; Pauly et al., 2011). In this process, mobile elements are released from the glass (Singer and Banin, 1990; Stroncik and Schmincke, 2001; Pauly et al., 2011) and eventually form secondary minerals, such as clay minerals, zeolites and carbonates (Nayudu, 1964; Fisher and Schmincke, 1984; Walton and Schiffman, 2003; Pauly et al., 2011). Immobile elements become passively enriched (Stroncik and Schmincke, 2001). Palagonite may thus be considered as a residual material, containing both amorphous and microcrystalline phases, that remains after selective dissolution of the initial basaltic parent glass (Thorseth et al., 1991; Drief and Schiffman, 2004). The process of glass alteration and palagonitization can occur both abiotically, through purely geochemical processes, and also through microbial activity (Thorseth et al., 1992; Staudigel et al., 2008; Pedersen et al., 2015; Türke et al., 2015).

Previous studies have shown that palagonitization rates are strongly dependent on temperature, with the process proceeding more rapidly at higher temperatures (Furnes, 1975; Jakobsson, 1978; Jakobsson and Moore, 1986; Singer and Banin, 1990). Other important factors that affect the process of palagonitization are porosity and water-rock ratio, fluid chemistry (including dissolved species, salinity and pH), fluid flow and original glass composition (Moore, 1966; Jakobsson and Moore, 1986; Stroncik and Schmincke, 2002; Crovisier et al., 2003; Pauly et al., 2011). As a result, palagonite does not have a single fixed composition, but rather its specific chemical composition and the type of secondary mineral phases, that may form from it, are strongly dependent on the abovementioned parameters. For this reason, the name "palagonite" is to be taken as a descriptive expression, which designates the product of a specific alteration process, rather than being a strictly defined term for a chemically well constrained phase, as it may describe both crystalline and amorphous material of varying composition (e.g. Staudigel and Hart, 1983). In addition, palagonite is known to change its composition and structure as it ages due to progressive devitrification and diffusive processes (Thorseth et al., 1991; Stroncik and Schmincke, 2001; Pauly et al., 2011). Due to the ambiguity of the term some authors, such as Honnorez (1978) have opted to forego the word palagonite entirely, in favor of the broader designation of "palagonitized glass".

Many previous investigations have focused on palagonitization in a relatively low-temperature environment, with studies on hydrothermal palagonitization rates being less common. Since palagonitization under non-hydrothermal diagenetic conditions tends to be a relatively slow process, with estimated palagonitization rates typically ranging between a few 10^{-3}–10^{-2} $\mu m \cdot yr^{-1}$ (Hekinian and Hoffert, 1975; Walton and Schiffman, 2003; Pauly et al., 2011), many aspects of palagonitization and the evolution of the resulting secondary mineral assemblages over time remain poorly understood. In this regard, the volcanic island of Surtsey, with its low-temperature meteoric to seawater dominated hydrothermal system, offers a unique opportunity to study palagonitization and its resulting authigenic smectite/zeolite/tobermorite mineral assemblage over time. The hydrothermal system at Surtsey is hypothesized to have initiated in response to heating by the basaltic intrusions that fed lava flows from 1964 to 1967 (Friedman and Williams, 1970; Jakobsson and Moore, 1982, 1986; Stefánsson et al., 1985). Since this time, the vitric basaltic tephra deposits have been undergoing progressive hydrothermal alteration, through the diverse processes that produce palagonitization of basaltic glass and cementation of the deposits by authigenic minerals (Fig. 1).

The first Surtsey drill core, SE-01, was retrieved in 1979 from the vicinity of the island's southeastern vent, *Surtur* (Fig. 2). Investigations of the 181 m long core by Jakobsson and Moore (1986) indicated that palagonitization of Surtsey tephra deposits is influenced by hydrothermal processes and varies with temperature. Below sea level alteration rims of smectitic clay mineral, mainly nontronite, were found to form around olivine crystal fragments. The thicknesses of these rims, much like the thicknesses of palagonitization rims on basaltic glass particles, were positively correlated with temperature.

A 192 m long drill core, SE-02b, was recovered at about 7 m lateral distance from SE-01 (Fig. 2) by the International Continental Scientific Drilling Program (ICDP) SUSTAIN project in 2017 (Jackson et al., 2019a; Weisenberger et al., 2019). The new core will allow us to build upon the prior research by Jakobsson and Moore (1986) to investigate how alteration of basaltic tephra in a low-temperature, hydrothermal system varies as a function of time, depth and temperature. For this purpose, the archived 1979 Surtsey drill core is revisited for petrographic analysis and a comparison is made with observations from corresponding depths of the 2017 drill core. The goal of this study is to evaluate and quantify changes in secondary mineralization, palagonitization and lithification of the Surtsey tephra, to characterize time-lapse alteration and constrain alteration rates. The petrographic results obtained from this study form the groundwork for future geochemical investigations of the Surtsey drill cores.

2. Geological setting

Surtsey is the youngest and southernmost member of the Vestmannaeyjar archipelago, which marks the seaward extension of Iceland's East Volcanic Zone (Moore, 1985; Jackson et al., 2015; Schipper et al., 2016) (Fig. 2). First emerging from the ocean surface on November 15, 1963, Surtsey was subsequently built up until June 5, 1967 by an interplay of early stage phreatomagmatic and mid to late stage effusive volcanism (Jakobsson and Moore, 1982). The eruption that formed the island took place in several episodes along a 4.5 km long ENE-trending array of five NNE-trending short submarine volcanic fissures approximately 33 km off Iceland's southern coast (Thorarinsson et al., 1964; Moore, 1985). Two smaller edifices, *Syrtlingur* and *Jólnir* developed, but were subsequently eroded (Jakobsson and Moore, 1982; Moore, 1985). Another volcanic ridge, *Surtla*, formed on the seafloor, between late December 1963 and early January 1964, but did not grow large enough to rise above sea level. On Surtsey an estimated amount of 0.7–0.8 km^3 of very poorly sorted, alkali-basaltic, glassy tephra was emplaced as bedded air fall and base surge deposits primarily via explosive discharge (cock's tails) and continuous uprush (tephra fingers) (Thorarinsson, 1965; Jakobsson and Moore, 1982). These deposits make up 60–70 vol% of all erupted material on Surtsey with the remaining fraction composed of crystalline alkali basalt, reworked sediments and sand/tephra layers at depths ≥118.5 m below sea level (Lorenz, 1974; Jakobsson and Moore, 1982).

One year after the cessation of volcanic activity, the first signs of an incipient hydrothermal system were observed in the form of visible

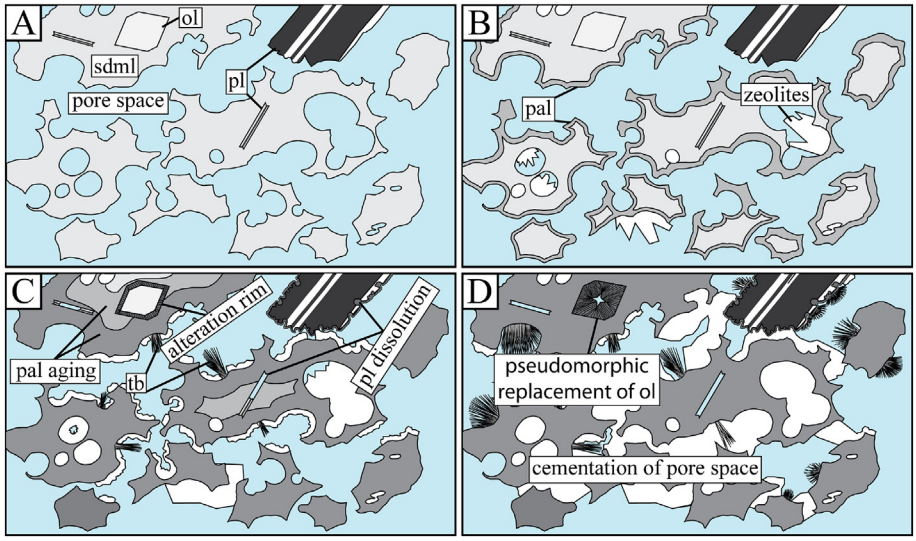

Fig. 1. Schematic outline of progressive alteration of vitric tephra deposits at Surtsey: A) Fresh, unaltered tephra, composed of sideromelane (sdml) and containing (micro-)phenocrysts of primary minerals, principally olivine (ol) and plagioclase (pl). B) Incipient stage of palagonitization, marked by the presence of thin amorphous gel-palagonite rims and scattered zeolite surface coatings. C) Progression of palagonitization with ongoing glass alteration and maturation of gel-palagonite rims. Zeolite cements become increasingly widespread and tobermorite (tb) begins to crystallize. Plagioclase dissolves, forming a thin coating of phyllosilicate minerals on the surface of larger crystals, while smaller crystals dissolve and leave voids within palagonitized glass. Below water level clay minerals form rims around olivine crystals and progressively encroach over time. D) More advanced alteration, most sideromelane has undergone palagonitization and most olivine grains have been altered to clay minerals. Cementation of the pore space is extensive, leading to a high degree of consolidation of the tuff and fortifying the material against erosion. The width of each image corresponds to about 5 mm. Mineral Abbreviations, where applicable, after Whitney and Evans (2010).

steam rising from the tephra pile and a zone of anomalous heat exchange (Friedman and Williams, 1970). The nature of hydrothermal processes on the island and associated alteration of the tephra deposits have been subject to earlier detailed studies (e.g. Jakobsson, 1972, 1978; Jakobsson and Moore, 1986; Jakobsson et al., 2000). In 1969, the first signs of palagonitization of the basaltic glass fraction of the tephra became evident and by 1976 most tephra within the thermal zone had undergone palagonitization (Jakobsson, 1971, 1972, 1978). Hydrothermal alteration of vitric basaltic tephra by palagonitization together with the formation of natural secondary mineral cements, have been recognized as key factors to the island's resistance to erosion, by causing the lithification of the tephra deposits (Jakobsson et al., 2000; Jackson et al., 2015; Romagnoli and Jakobsson, 2015). In addition, Surtsey has been recognized as having a secondary mineral assemblage that is unique in both the Vestmannaeyjar archipelago as well as in greater Iceland (Jakobsson and Moore, 1986; Jackson et al., 2019b).

3. The Surtsey hydrothermal system

The hydrothermal system at Surtsey is characterized by several distinct hydrological zones. The uppermost zone above the water table is dominated by meteoric fluids that are derived from rainwater. Surface vapors indicate that this depth interval contains steam zones.

The water table, which is influenced by tidal fluctuations, is located at ca. 58 m measured depth for the two studied drill cores (Weisenberger et al., 2019). Geophysical borehole logging conducted after drilling of SE-02b indicates a freshwater lens at this depth (Jackson et al., 2019a; Weisenberger et al., 2019). The exact thickness of the lens remains unclear since fluids in the borehole were still disturbed due to drilling when the measurements were conducted. The freshwater lens overlies more saline fluids of modified seawater composition (Jackson et al., 2019a).

Temperature profiles obtained over the course of 37 years show, that the system has gradually undergone cooling (Fig. 3). The system's temperature maximum occurs at a vertical depth of about 105–110 m below the surface for the two vertical boreholes considered in this study. Temperature at this depth has decreased from 141 °C in 1980 to 124 °C in 2019. The temperature logs indicate a cooling point at a depth of about 145 m below the surface, which likely represents a cold inflow zone (Weisenberger et al., 2019; Jackson et al., 2019a).

4. Methods and materials

4.1. Thin section petrography

Petrographic thin sections were prepared for samples from the archive of the SE-01 drill core, stored in core boxes at ambient temperatures since 1979, and the SE-02b drill core. All SE-01 thin sections as well as reference samples from the SE-02b core (see Weisenberger et al., 2019) were prepared using yellow epoxy resin. An additional series of thin sections from the SE-02b core was prepared from selected research samples using blue epoxy resin. All samples were soaked in epoxy resin prior to polishing, due to the fragility and friable nature of the sample material. Heating the epoxy resin above 50 °C was avoided in all thin sections in order to preserve temperature-sensitive hydration. Table 1 provides an overview of selected samples for this study.

Primary mineral phases and authigenic features, such as altered glass and secondary minerals, were quantified by point counts, using a step interval of 0.18 mm. The number of counted points was dependent on the individual sample and ranged from 603 to 4557 points, with an average number of counts per sample of 2322. The degree of palagonitization was determined as the fraction of basaltic glass (sideromelane) in a sample, which has become palagonitized, given as

$$\frac{V_{\text{palagonitized glass}}}{(V_{\text{palagonitized glass}} + V_{\text{glass}})} \cdot 100\text{vol}\%$$

where $V_{\text{palagonitized glass}}$ and V_{glass} refer to the total volume of palagonitized glass and sideromelane within a given thin section as indicated by point counts. Thicknesses of alteration rims (i.e. palagonitized glass and clay mineral rims around olivine) were obtained by conducting as many measurements as possible by use of a petrographic microscope followed by determination of median values for each sample. Sideromelane was identified purely based on its distinct coloration as well as its optical isotropy (complete extinction under cross-polarized light). However, as a recent study by Jackson et al., (2019b) has demonstrated, such seemingly unaltered glasses may also

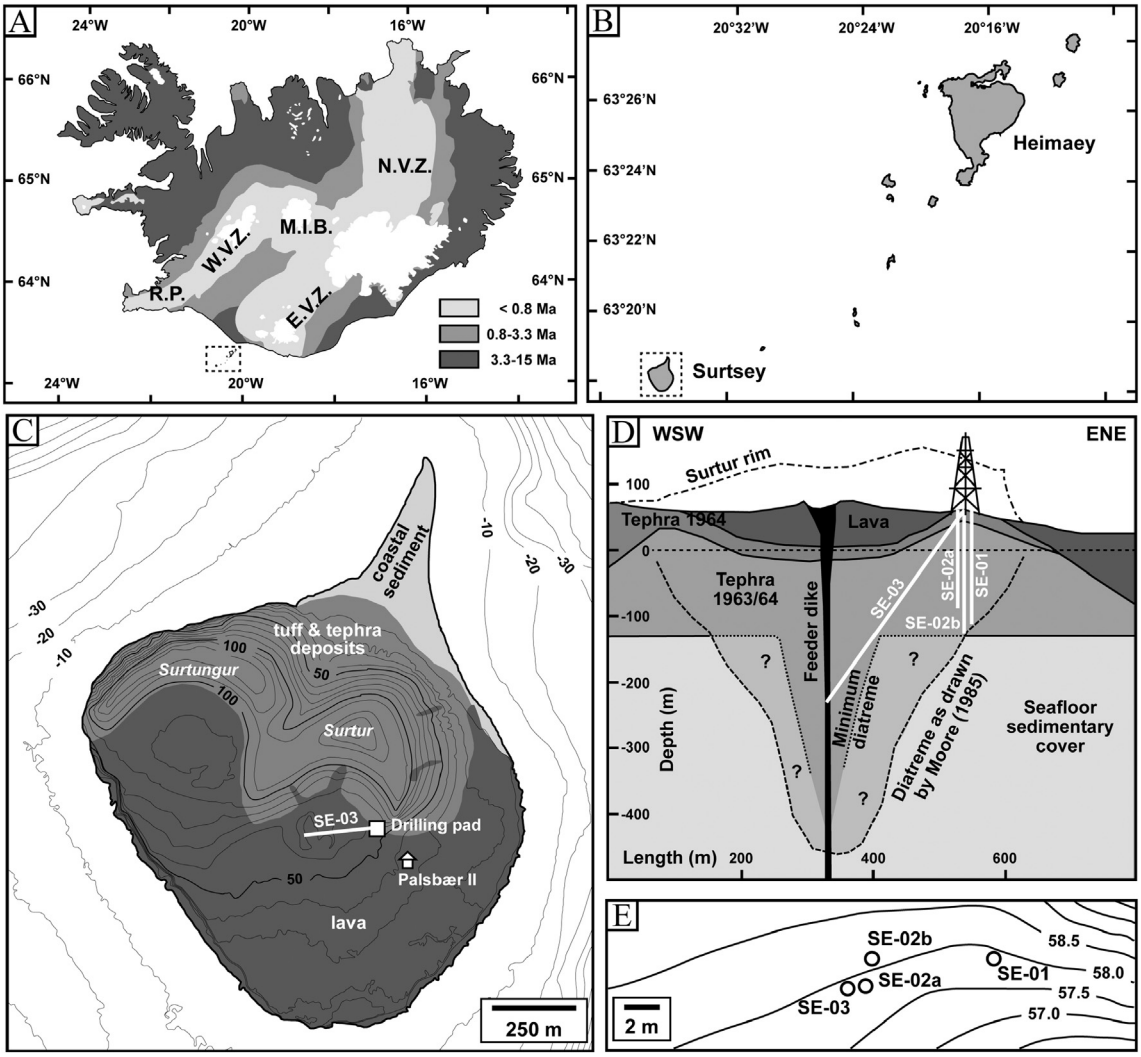

Fig. 2. Overview of Surtsey and the 1979 and 2017 drilling projects. A) Simplified geologic map showing the age distribution of rocks in greater Iceland in Ma and the main volcanic provinces (N.V.Z: North Volcanic Zone, M.I.B.: Mid-Iceland Belt, W.V.Z.: West Volcanic Zone, E.V.Z.: East Volcanic Zone, R.P.: Reykjanes Peninsula). The Vestmannaeyjar archipelago (dashed rectangle) marks the southern seaward extension of the E.V.Z. B) The Surtsey eruptions form the southernmost extension of the archipelago. C) Geologic map of Surtsey highlighting the position of the drill pad and the Pálsbær II hut. D) Schematic cross-section through the Surtur tuff cone showing depth and orientation of the boreholes as well as the island's subsurface structure, based on Moore (1985). The drill holes from 1979 (SE-01) and 2017 (SE-02a, SE-02b and SE-03) are situated in close proximity at the eastern edge of the Surtur tephra pile. E) The relative position of the boreholes. After Jackson et al., (2019a) and Weisenberger et al. (2019).

contain nanocrystalline clay minerals, which are unobservable under the microscope. Here we use the term "sideromelane" to refer to the fraction of glassy lapilli, which appears unaltered based purely on optical microscopy.

4.2. X-ray powder diffraction

X-ray powder diffraction (XRPD) analysis was performed on samples of the 1979 core (SE-01) in order to confirm the results of the point count data. XRD analyses were carried out using a Panalytical X'Pert Pro diffractometer (RTMS X'Celerator detector) and Bruker D2 Phaser (LINKEYE detector) diffractometer at the Department of Earth Sciences, Environment and Resources (DiSTAR) of the University of Naples Federico II.

The following operative conditions were used: CuKα radiation, 40 kV, 40 mA, 2ϑ range from 4 to 70°, equivalent step size 0.017° 2ϑ, 30 s per step counting time for X'Pert Pro; CuKα radiation, 30 kV, 15 mA, 2ϑ range from 4 to 70°, 0.02 2ϑ step size, 66 s per step counting time for Bruker D2 Phaser. The analyses were used to obtain a calibration between the two different diffractometers. Each sample was disaggregated by hand in an agate mortar to obtain a homogeneous powder (particle size <200 μm). An amount of 20 wt% corundum (α-Al_2O_3, Buehler micropolish, 1 μm grain size) was added as an internal standard. This mixture was subsequently micronized (grain size <10 μm) by using a McCrone Micronising Mill, with agate cylinders and 10 mL of deionized water for 15 min of grinding time. This technique was used to reduce preferred orientation, primary extinction or crystallite size issues which commonly affect clay minerals (Bish and Chipera, 1987). For the qualitative interpretations of XRPD patterns the Panalytical HighScore Plus 3.0d software was used, while BRUKER TOPAS 5.0 software was employed for quantitative evaluations with the combined RIR/Rietveld approach.

4.3. Surtsey drill cores

Two drill cores have been selected for this study: SE-01 and SE-02b (Fig. 2). The studied drill core samples, except for the samples obtained from crystalline basalt, can universally be described as hypocrystalline (lapilli-) tuff of inequigranular grain size distribution at different stages of palagonitization, which contains varying amounts of secondary minerals associated with palagonitic glass alteration. The principal constituents of the samples are angular to slightly rounded ash to lapilli-sized

fragments of sideromelane. The outline given below is only intended as a very brief overview of macroscopic lithological characteristics. For a more comprehensive description of the 1979 and 2017 Surtsey drill cores the reader is referred to Jakobsson and Moore (1982) and Weisenberger et al. (2019).

4.3.1. SE-01

Above water level the tuff is beige to brown in color and remains poorly altered. The degree of consolidation is typically low. Some primary layering may be observed locally. At 55.3 m, which is close to the uppermost tidal dominated water level, the first macroscopically visible signs of alteration in the form of white mineral cements in pore space become apparent. These increase in abundance downcore, leading to a progressive reduction of estimated pore space with depth as the rock begins to take on a greenish hue and increases in hardness and density, as inferred by weight. Between 72.3 and 83.4 m a basaltic intrusion is present. The tuff is more poorly consolidated and friable in the zone between ca. 139.3–150.3 m, locally leading to poor core recovery between 140.0–143.8 and 148.5–150.3 m. Below this depth, the material becomes slightly more consolidated up until 157.3 m. Below 157.3 m core recovery was again poor with the recovered tuff being dark gray in coloration as well as very friable. Alteration mineralogy at this depth consists mainly of anhydrite, which occurs as a macroscopically visible white to translucent phase in the pore space and along fractures. Between 170.5 and 180.1 m only cuttings were recovered.

4.3.2. SE-02b

Armored lapilli were locally described above water level as well as down to ca. 62.6 m depths (Weisenberger et al., 2019). The basaltic intrusion found in SE-01 at 72.3–83.4 m depths is not present in SE-02b, despite the horizontal distance between the cores being <7 m, possibly indicating a complex geometry of the intrusive body. Unlike in SE-01, fully consolidated core material was recovered from the area between 139.3–150.3 m and below 157.3 m. Despite this, the tuff remains poorly altered in the depth interval between 138.4 and 150.3 m. Here the main secondary minerals are anhydrite, gypsum and calcite, rather than zeolites or tobermorite, which dominate in the more strongly altered zones. Estimated porosities (Table 1) for this poorly altered zone are high, reaching up to 38.6 vol%. The tuff in the depth interval below 150 m down to 178 m is more consolidated and shows extensive signs of alteration in the form of macroscopically visible cementation and darkened coloration as well as palagonitization. Below 178 m the rock remains poorly altered and very friable.

5. Results

5.1. Primary phases

The primary crystalline phases present in the Surtsey tuff samples are plagioclase, clinopyroxene and olivine. These occur as (micro-) phenocrysts in the glassy particles and as crystal fragments. Minor amounts of opaque phases are present as well. A brief description of the primary phases is given below.

5.1.1. Sideromelane

Sideromelane appears in thin section as a vesicular bright yellow to pink gel-like phase containing sporadic phenocrysts of plagioclase, olivine and clinopyroxene. It is distinguished from palagonitized glass mainly by its characteristic color, as opposed to the darker reddish brown of type I palagonitization rims (see Section 5.2.1 Palagonitized glass). Furthermore, the complete optical isotropy of sideromelane makes it distinct from type II and III palagonitized glass. Despite this seemingly obvious distinction, it should be noted that "fresh" sideromelane is identified here under purely optical criteria and thus some alteration of the glass may have occurred on a microscale. Since submicroscopic nanocrystalline phases, such as clay minerals, as identified by Jackson et al., (2019b), cannot be identified by optical microscopy, our definition of "sideromelane" cannot possibly account for their presence.

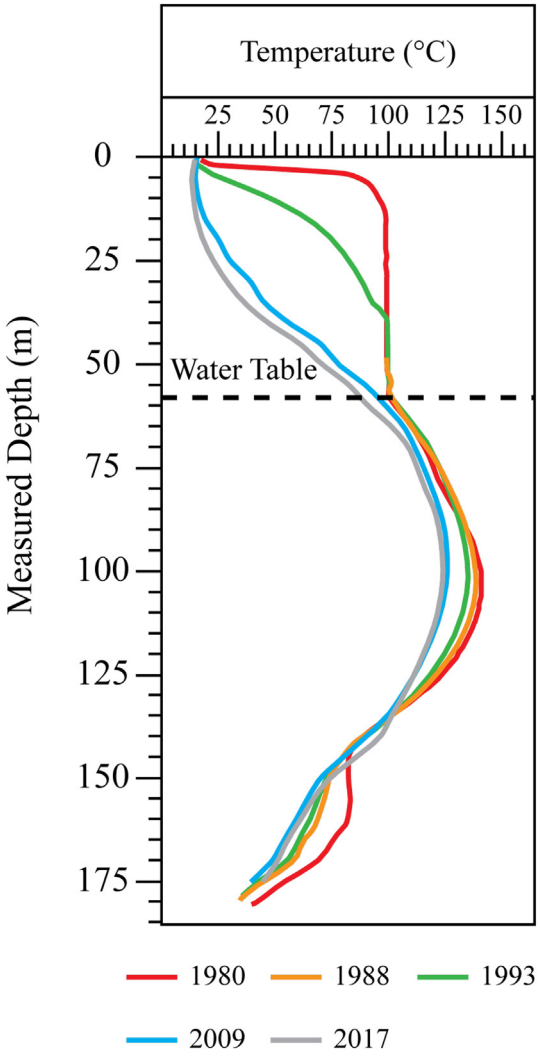

Fig. 3. Borehole temperature profiles for SE-01 obtained between 1980 and 2017 by downholelogging.

5.1.2. Plagioclase

Plagioclase typically occurs in the form of anhedral, single crystals or granular aggregates with an average grainsize between 150 and 200 μm, typically forming a microlitic texture within sideromelane. Some rare larger phenocrysts of up to 1 cm can be found in the Surtsey lapilli-tuff. Both above and below water level some of these larger massive phenocrysts show minor signs of dissolution in the form of serrated or frayed grain boundaries and occasional low amounts of secondary clay mineral formation. Smaller plagioclase microphenocrysts generally decrease in abundance within the temperature maximum of the system at 105–110 m, leaving behind voids in glass upon their dissolution. According to XRPD, the amount of plagioclase in the tuff lies between 2 and 19 wt% with an average of 9 wt% (Grimaldi, 2018).

5.1.3. Clinopyroxene

Clinopyroxene is very common in the Surtsey tephra, making up a fraction between 2 and 9 wt% (average: 6 wt%) of the phases identified in the tuff samples by XRPD (Grimaldi, 2018). It occurs in the form of anhedral granular to columnar microphenocrysts in sideromelane. These typically have an average size of about 230 μm.

Table 1
Samples and petrographic results from optical thin section microscopy.

Drill hole	Depth (m)	IGSN #	Rock type	Sample type	Primary minerals (vol%)	Glass Alteration (vol%)		Secondary minerals (vol%)					Porosity (vol%)	Degree of palagonitization (vol%)	Palagonitization extent[b] (vol%)	Rim thickness (μm)	
					(Pl + Cpx + Ol)[a]	Sdml[a]	Pal[a]	Php[a]	Anl[a]	Tb[a]	Anh[a]	Gp[a]				Pal[a]	Ol[a]
SE-01	4.9	–	Lapilli-Tuff	Core	4.5	9.7	42.9	3.1	8.6	0.0	0.2	n.a.	31.1	81.5	84.9	75.0	0.0
SE-01	22.0	–	Lapilli-Tuff	Core	3.2	12.8	35.1	5.5	4.1	0.3	1.4	n.a.	37.6	73.3	77.9	120.0	0.0
SE-01	43.6	–	Lapilli-Tuff	Core	2.4	48.5	13.4	1.2	0.0	0.3	0.3	n.a.	33.9	21.6	23.5	8.8	0.0
SE-01	55.8	–	Lapilli-Tuff	Core	4.6	10.0	46.8	3.5	1.4	5.0	0.3	n.a.	28.4	82.4	85.0	75.0	0.0
SE-01	65.4	–	Lapilli-Tuff	Core	4.7	2.2	47.7	4.5	7.8	2.4	0.4	n.a.	30.2	95.5	96.5	240.0	0.0
SE-01	72.4	–	Lapilli-Tuff	Core	5.6	0.0	57.6	10.2	0.0	0.0	0.5	n.a.	26.2	100.0	100.0	n.a.	30.0
SE-01	72.4	–	Crystalline basalt	Core	95.1	0.0	0.0	0.0	0.0	1.9	1.0	n.a.	2.0	n.a.	n.a	n.a.	n.a.
SE-01	76.1	–	Crystalline basalt	Core	96.4	0.0	0.0	0.0	0.0	0.1	0.0	n.a.	3.6	n.a.	n.a.	n.a.	n.a.
SE-01	83.5	–	Crystalline basalt	Core	96.1	0.0	0.0	0.0	0.0	0.4	1.3	n.a.	2.1	n.a.	n.a.	n.a.	n.a.
SE-01	83.5	–	Lapilli-Tuff	Core	3.7	0.0	57.9	1.2	10.4	0.0	5.3	n.a.	21.5	100.0	100.0	n.a.	70.0
SE-01	86.6	–	Lapilli-Tuff	Core	3.8	0.3	53.4	1.7	6.7	5.3	2.2	n.a.	26.6	99.5	99.6	510.0	70.0
SE-01	90.1	–	Lapilli-Tuff	Core	1.4	0.0	56.7	5.7	2.6	6.7	0.9	n.a.	26.0	100.0	100.0	n.a.	60.0
SE-01	92.6	–	Lapilli-Tuff	Core	3.1	0.0	55.7	0.8	7.8	5.2	1.4	n.a.	26.0	100.0	100.0	n.a.	75.0
SE-01	95.4	–	Lapilli-Tuff	Core	15.3	26.4	35.4	1.7	1.8	3.7	0.0	n.a.	15.8	57.3	61.7	n.a.	50.0
SE-01	95.5	–	Lapilli-Tuff	Core	3.7	2.9	64.4	1.6	2.1	7.8	0.0	n.a.	17.5	95.7	96.4	257.5	n.a.
SE-01	95.6	–	Lapilli-Tuff	Core	3.3	0.2	52.3	0.8	9.7	0.1	12.8	n.a.	20.9	99.6	99.7	420.0	n.a.
SE-01	105.0	–	Lapilli-Tuff	Core	3.8	0.0	52.3	1.2	3.7	7.1	4.3	n.a.	27.6	100.0	100.0	n.a.	60.0
SE-01	111.0	–	Lapilli-Tuff	Core	0.9	0.6	61.5	2.7	6.1	1.6	0.1	n.a.	26.6	99.0	99.2	440.0	95.0
SE-01	120.6	–	Lapilli-Tuff	Core	3.6	1.5	56.1	0.6	6.4	4.5	0.1	n.a.	27.2	97.3	97.8	360.0	50.0
SE-01	137.8	–	Lapilli-Tuff	Core	11.2	14.0	41.0	9.6	2.4	3.9	0.2	n.a.	17.7	74.6	80.3	120.0	25.0
SE-01	140.0–141.0	–	Lapilli-Tuff	Cuttings	n.a.	n.a.	n.a.	n.a.	n.a.	n.a.	n.a.	n.a.	n.a.	n.a.	n.a.	0.0	0.0
SE-01	143.0–144.0	–	Lapilli-Tuff	Cuttings	n.a.	n.a.	n.a.	n.a.	n.a.	n.a.	n.a.	n.a.	n.a.	n.a.	n.a.	0.0	0.0
SE-01	148.0–149.0	–	Lapilli-Tuff	Cuttings	n.a.	n.a.	n.a.	n.a.	n.a.	n.a.	n.a.	n.a.	n.a.	n.a.	n.a.	0.0	0.0
SE-01	148.3	–	Lapilli-Tuff	Core	5.4	43.3	24.6	8.1	0.0	0.0	0.7	n.a.	17.9	36.2	43.0	40.0	0.0
SE-01	149.0–150.0	–	Lapilli-Tuff	Cuttings	n.a.	n.a.	n.a.	n.a.	n.a.	n.a.	n.a.	n.a.	n.a.	n.a.	n.a.	0.0	0.0
SE-01	150.3	–	Lapilli-Tuff	Core	5.4	47.8	15.2	5.9	0.2	0.0	2.5	n.a.	23.1	24.1	30.8	40.0	0.0
SE-01	156.9	–	Lapilli-Tuff	Core	7.4	23.2	43.8	3.0	2.0	2.7	0.0	n.a.	18.0	65.4	69.0	50.0	20.0
SE-01	157.3–158.0	–	Lapilli-Tuff	Cuttings	n.a.	n.a.	n.a.	n.a.	n.a.	n.a.	n.a.	n.a.	n.a.	n.a.	n.a.	0.0	0.0
SE-01	165.0–166.0	–	Lapilli-Tuff	Cuttings	n.a.	n.a.	n.a.	n.a.	n.a.	n.a.	n.a.	n.a.	n.a.	n.a.	n.a.	0.0	0.0
SE-01	169.5	–	Lapilli-Tuff	Core	4.0	55.7	0.0	0.0	0.0	0.0	19.6	n.a.	20.6	0.0	0.0	0.0	0.0
SE-01	176.5–177.7	–	Lapilli-Tuff	Cuttings	n.a.	n.a.	n.a.	n.a.	n.a.	n.a.	n.a.	n.a.	n.a.	n.a.	n.a.	0.0	0.0
SE-01	178.7–180.1	–	Lapilli-Tuf	Cuttings	n.a.	n.a.	n.a.	n.a.	n.a.	n.a.	n.a.	n.a.	n.a.	n.a.	n.a.	0.0	0.0
SE-02b	13.2	ICDP5059EX3J001	Lapilli-Tuff	Core	5.6	18.3	31.4	6.8	5.6	0.0	0.9	0.0	31.4	63.1	70.5	52.5	0.0
SE-02b	22.6	ICDP5059EX1A701	Lapilli-Tuff	Core	6.9	7.5	43.6	6.8	10.9	3.4	0.9	0.0	20.0	85.3	89.6	135.0	0.0
SE-02b	31.2	ICDP5059EX7J001	Lapilli-Tuff	Core	5.8	9.5	44.1	5.2	9.8	3.6	0.1	1.1	20.7	82.2	86.8	132.5	0.0
SE-02b	34.8	ICDP5059EXBA701	Lapilli-Tuff	Core	5.2	11.5	39.3	5.0	5.6	9.3	1.4	0.0	22.6	77.4	83.8	n.a.	0.0
SE-02b	40.4	ICDP5059EX8J001	Lapilli-Tuff	Core	6.6	9.7	52.7	4.8	4.3	3.8	0.2	0.2	17.7	84.4	87.1	90.0	0.0
SE-02b	43.7	ICDP5059EXLA701	Lapilli-Tuff	Core	6.8	9.4	38.6	9.4	2.7	5.1	0.3	0.0	27.7	80.4	85.6	150.0	0.0
SE-02b	56.0	ICDP5059EXVA701	Lapilli-Tuff	Core	3.9	8.5	46.2	4.1	3.3	6.0	0.4	0.0	27.7	84.5	87.6	145.0	0.0
SE-02b	56.1	ICDP5059EXGJ001	Lapilli-Tuff	Core	5.2	4.7	44.7	6.5	12.6	5.4	0.0	0.0	20.8	90.4	93.6	260.0	0.0
SE-02b	58.9	ICDP5059EXHJ001	Lapilli-Tuff	Core	n.a.	n.a.	n.a.	n.a.	n.a.	n.a.	n.a.	n.a.	n.a.	n.a.	n.a.	480.0	0.0

SE-02b	62.1	ICDP5059EXIJ001	Lapilli-Tuff	Core	5.1	1.2	49.1	6.9	9.6	7.2	0.0	0.0	20.9	97.6	98.3	n.a.	20.0
SE-02b	65.4	ICDP5059EX5B701	Lapilli-Tuff	Core	4.3	0.3	52.7	4.4	14.1	6.3	0.0	0.0	17.9	99.4	99.6	n.a.	30.0
SE-02b	67.5	ICDP5059EXJJ001	Lapilli-Tuff	Core	n.a.	n.a.	n.a.	n.a.	n.a.	n.a.	n.a.	n.a.	n.a.	n.a.	n.a.	430.0	60.0
SE-02b	70.1	ICDP5059EXLJ001	Lapilli-Tuff	Core	n.a.	n.a.	n.a.	n.a.	n.a.	n.a.	n.a.	n.a.	n.a.	n.a.	n.a.	420.0	80.0
SE-02b	75.0	ICDP5059EXMJ001	Lapilli-Tuff	Core	n.a.	n.a.	n.a.	n.a.	n.a.	n.a.	n.a.	n.a.	n.a.	n.a.	n.a.	400.0	70.0
SE-02b	78.4	ICDP5059EXFB701	Lapilli-Tuff	Core	9.2	0.5	51.3	2.9	9.6	5.7	0.1	0.0	20.6	99.1	99.3	n.a.	n.a.
SE-02b	80.5	ICDP5059EXNJ001	Lapilli-Tuff	Core	n.a.	n.a.	n.a.	n.a.	n.a.	n.a.	n.a.	n.a.	n.a.	n.a.	n.a.	n.a.	72.5
SE-02b	86.5	ICDP5059EXPB701	Lapilli-Tuff	Core	2.3	0.0	61.4	1.2	12.6	3.9	0.0	0.0	18.5	99.9	99.9	n.a.	125.0
SE-02b	87.8	ICDP5059EXOJ001	Lapilli-Tuff	Core	n.a.	n.a.	n.a.	n.a.	n.a.	n.a.	n.a.	n.a.	n.a.	100.0	n.a.	n.a.	150.0
SE-02b	89.2	ICDP5059EXPJ001	Lapilli-Tuff	Core	n.a.	n.a.	n.a.	n.a.	n.a.	n.a.	n.a.	n.a.	n.a.	100.0	n.a.	n.a.	107.5
SE-02b	89.5	ICDP5059EXQJ001	Lapilli-Tuff	Core	n.a.	n.a.	n.a.	n.a.	n.a.	n.a.	n.a.	n.a.	n.a.	100.0	n.a.	n.a.	n.a.
SE-02b	92.6	ICDP5059EXZB701	Lapilli-Tuff	Core	2.0	0.0	56.2	0.1	18.1	1.8	0.3	0.0	21.5	100.0	100.0	n.a.	165.0
SE-02b	97.5	ICDP5059EXRJ001	Lapilli-Tuff	Core	n.a.	n.a.	n.a.	n.a.	n.a.	n.a.	n.a.	n.a.	n.a.	100.0	n.a.	n.a.	150.0
SE-02b	101.5	ICDP5059EX9C701	Lapilli-Tuff	Core	1.5	0.0	58.0	0.4	15.7	2.4	0.9	0.0	21.1	100.0	100.0	n.a.	175.0
SE-02b	106.1	ICDP5059EXSJ001	Lapilli-Tuff	Core	n.a.	n.a.	n.a.	n.a.	n.a.	n.a.	n.a.	n.a.	n.a.	100.0	n.a.	n.a.	n.a.
SE-02b	111.0	ICDP5059EXJC701	Lapilli-Tuff	Core	1.8	0.0	67.5	2.0	10.0	6.5	0.3	0.0	12.0	100.0	100.0	n.a.	160.0
SE-02b	120.8	ICDP5059EXTC701	Lapilli-Tuff	Core	3.4	0.0	68.4	0.4	5.4	6.6	0.0	0.0	15.8	100.0	100.0	n.a.	n.a.
SE-02b	121.4	ICDP5059EXUJ001	Lapilli-Tuff	Core	n.a.	n.a.	n.a.	n.a.	n.a.	n.a.	n.a.	n.a.	n.a.	100.0	n.a.	n.a.	n.a.
SE-02b	128.0	ICDP5059EX3D701	Lapilli-Tuff	Core	1.1	0.0	59.7	0.8	17.8	3.7	0.1	0.0	16.8	100.0	100.0	n.a.	n.a.
SE-02b	134.3	ICDP5059EXVJ001	Lapilli-Tuff	Core	5.4	0.0	60.5	0.8	15.0	3.1	0.0	0.0	15.2	100.0	100.0	n.a.	50.0
SE-02b	138.4	ICDP5059EXDD701	Lapilli-Tuff	Core	3.7	1.2	61.0	2.9	8.6	7.3	0.2	0.0	15.2	98.0	98.5	410.0	32.5
SE-02b	141.5	ICDP5059EXWJ001	Lapilli-Tuff	Core	3.9	16.4	39.2	9.3	1.9	0.0	10.4	0.0	18.9	70.6	75.5	n.a.	0.0
SE-02b	142.6	ICDP5059EXXJ001	Lapilli-Tuff	Core	4.4	48.6	0.0	0.0	0.0	0.0	7.2	1.2	38.6	0.0	0.0	0.0	0.0
SE-02b	144.1	ICDP5059EXYJ001	Lapilli-Tuff	Core	5.3	57.9	0.0	0.0	0.0	0.0	1.0	4.3	31.5	0.0	0.0	0.0	0.0
SE-02b	147.1	ICDP5059EXZJ001	Lapilli-Tuff	Core	10.2	53.3	9.5	0.1	0.1	0.0	1.0	1.0	24.8	15.2	15.5	22.5	0.0
SE-02b	148.7	ICDP5059EXND701	Lapilli-Tuff	Core	7.7	11.3	50.1	9.6	4.1	6.1	0.1	0.0	10.9	81.5	86.0	130.0	0.0
SE-02b	150.3	ICDP5059EX0K001	Lapilli-Tuff	Core	7.5	15.7	46.0	9.9	6.6	3.4	0.3	0.2	10.4	74.6	80.8	170.0	0.0
SE-02b	153.3	ICDP5059EX1K001	Lapilli-Tuff	Core	n.a.	n.a.	n.a.	n.a.	n.a.	n.a.	n.a.	n.a.	n.a.	n.a.	n.a.	n.a.	n.a.
SE-02b	157.5	ICDP5059EXXD701	Lapilli-Tuff	Core	5.3	0.0	62.6	3.0	10.2	5.6	1.1	0.0	12.3	99.9	99.9	n.a.	45.0
SE-02b	159.0	ICDP5059EX2K001	Lapilli-Tuff	Core	n.a.	n.a.	n.a.	n.a.	n.a.	n.a.	n.a.	n.a.	n.a.	n.a.	n.a.	480.0	25.0
SE-02b	165.6	ICDP5059EX7E701	Lapilli-Tuff	Core	9.5	0.4	64.0	1.5	6.8	5.0	0.1	0.0	12.7	99.4	99.5	480.0	50.0
SE-02b	168.1	ICDP5059EX3K001	Lapilli-Tuff	Core	n.a.	n.a.	n.a.	n.a.	n.a.	n.a.	n.a.	n.a.	n.a.	n.a.	n.a.	330.0	40.0
SE-02b	176.1	ICDP5059EXHE701	Lapilli-Tuff	Core	7.2	2.0	66.0	1.3	5.4	4.8	0.6	0.0	12.7	97.1	97.5	n.a.	n.a.
SE-02b	176.4	ICDP5059EX4K001	Lapilli-Tuff	Core	n.a.	n.a.	n.a.	n.a.	n.a.	n.a.	n.a.	n.a.	n.a.	n.a.	n.a.	340.0	35.0
SE-02b	177.8	ICDP5059EX5K001	Lapilli-Tuff	Core	8.6	5.1	55.3	1.3	7.0	14.3	0.0	0.0	8.3	91.6	93.9	215.0	20.0
SE-02b	180.9	ICDP5059EXRE701	Lapilli-Tuff	Core	10.5	51.3	0.5	0.0	0.0	0.0	0.2	0.0	37.4	1.0	1.0	n.a.	0.0
SE-02b	181.5	ICDP5059EX6K001	Lapilli-Tuff	Core	n.a.	n.a.	n.a.	n.a.	n.a.	n.a.	n.a.	n.a.	n.a.	0.0	n.a.	0.0	0.0

[a] Abbreviations: Pl: Plagioclase, Cpx: Clinopyroxene, Ol: Olivine, Sdml: Sideromelane, Pal: Palagonite, Php: Phillipsite, Anl: Analcime, Tb: Tobermorite, Anh: Anhydrite, Gp: Gypsum, n.a.: not analyzed.

[b] Palagonitization extent based on the method used by Pauly et al. (2011), calculated using relative quantities of authigenic phases and primary glass: (%Pal + %Php + %Anl + %Tb)/(%Sdml + %Pal + %Php + %Anl + %Tb) · 100%.

5.1.4. Olivine

Olivine commonly occurs as granular, massive and rarely prismatic anhedral to subhedral crystals. Very few euhedral crystals are present. Below water level olivine crystals are commonly rimmed by authigenic clay minerals. Within the zone of maximum temperature at 105–110 m (Weisenberger et al., 2019) unaltered olivine is uncommon and most crystals are altered to nanocrystalline clay mineral. At this depth, fresh unaltered olivine, as determined by XRPD, forms 0–3 wt% (average: 1 wt%) of the lapilli tuff (Grimaldi, 2018). Crystal size typically ranges between 200 and 600 μm, with some larger phenocrysts reaching up to 3 mm in diameter. The thickness of the alteration rims on olivine, much like that of the palagonitized glass rims, is positively correlated with temperature and has noticeably increased between 1979 and 2017 in samples from corresponding depths (Fig. 4).

5.2. Authigenic alteration phases

Alteration in both Surtsey drill cores is dominated by palagonitization of sideromelane and the formation of phillipsite, analcime as well as acicular tobermorite. Other secondary phases include clay minerals, which occur either as highly birefringent microcrystalline mineral aggregates in altered glass or as replacement rims on olivine, calcium sulphates (anhydrite, gypsum and bassanite), and calcite.

5.2.1. Palagonitized glass

Based on petrographic investigations of lapilli-sized fragments in thin sections of the archived 1979 Surtsey SE-01 drill core and the 2017 SE-02b drill core, we distinguish three principal types of palagonitic textures.

5.2.1.1. Type I (gel-palagonite). The altered glass falling into this category is clear, translucent and reddish brown in coloration (Fig. 5A). Its appearance is gel-like and amorphous to slightly crystalline (e.g. Stroncik and Schmincke, 2001, 2002). This type of palagonite commonly marks zones, where the degree of palagonitization is ≤80.0 vol%. Type I palagonitization rims are comparatively thin as well as optically isotropic.

5.2.1.2. Type II (fibro-palagonite). Type II altered glass (Fig. 5B) rims possess a grainy to fibrous texture. In plane polarized light they are reminiscent of type I rims, yet they may be slightly brighter in appearance. Rims belonging to this category are cryptocrystalline and show strong birefringence with colorful yellow, green and red interference colors, which strongly resemble those of clay minerals – a property, which sets them apart from type I palagonitized glass rims. Type II occurs in depth intervals of intermediate temperature. Between 1979 and 2017 type II has replaced type I at the lower end of the temperature spectrum and in turn has become replaced by type III palagonitized glass rims in depth intervals of comparatively higher temperatures.

5.2.1.3. Type III. Type III altered glass (Fig. 5C) occurs below water level in both drill cores. It is darkened, opaque and spotty rather than translucent in appearance. Interference colors are far less intense than in type II and in some instances the material might appear completely opaque under cross polarized light. In SE-01 this kind of palagonitization is only found close to the hydrothermal system's zone of maximum temperature. In SE-02b it has spread both upwards and downwards to become the dominant type of palagonitized glass between 67.5 and 134.3 m as well as being present together with type II below 153.3 m.

In instances, where different types appear together, most prominently in SE-02b between 150.3 and 177.8 m, they are generally concentrically arranged around sideromelane in the order of type III → type II → type I → sideromelane (Fig. 6).

5.2.2. Analcime

Analcime (general formula: $NaAlSi_2O_6 \cdot (H_2O)$) is the most abundant secondary mineral phase in terms of both volume and weight percentages according to XRPD and point counts in most of the samples. The

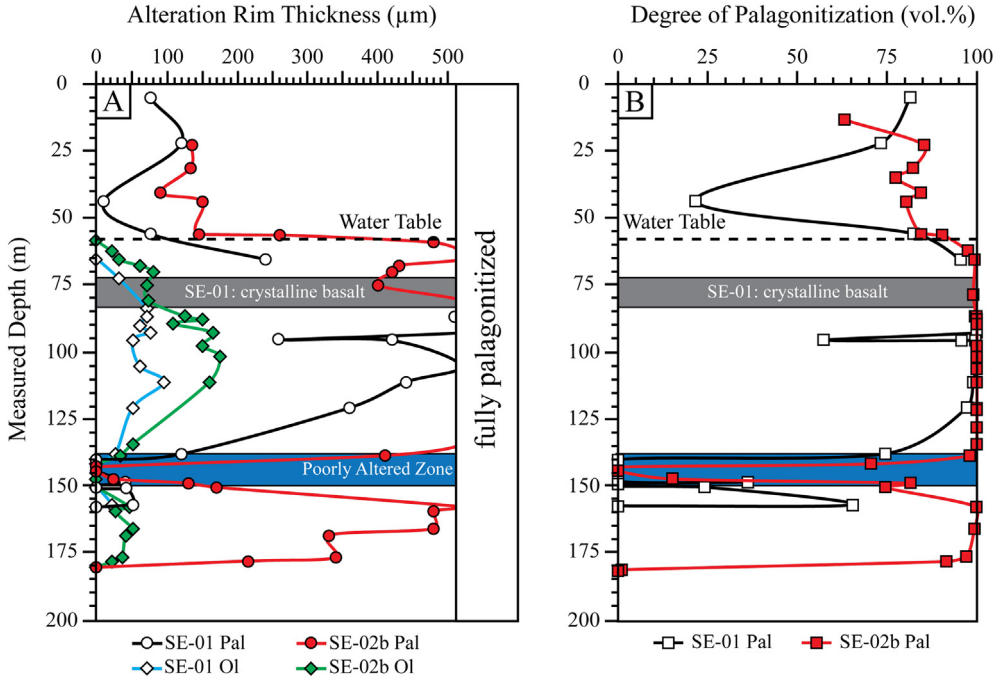

Fig. 4. A) Thicknesses of palagonitization rims on altered glass lapilli and clay mineral rims on olivine crystals in the archived 1979 SE-01 drill core and the 2017 drill core, SE-02b, plotted versus depth and measured through petrographic studies of thin sections. In both drill cores, several samples from the poorly altered zone contain neither palagonitic nor olivine rims. B) Comparison of the measured degree of palagonitization with depth between SE-01 and SE-02b.

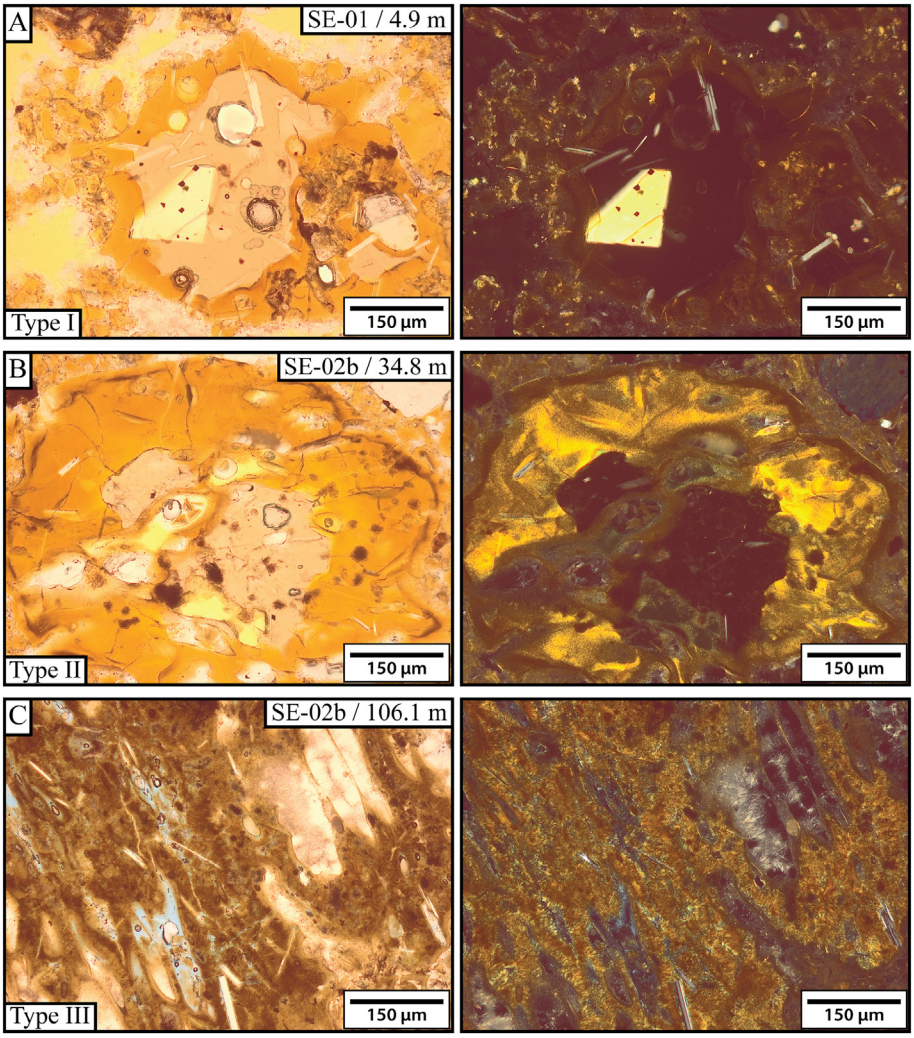

Fig. 5. Three different types of palagonitized glass recognized in the Surtsey samples. A) Type I, or gel-palagonite, is mainly isotropic and shows little to no birefringence. B) Type II, showing bright and high intensity interference colors reminiscent of clay minerals as well as a weakly granular to fibrous texture. C) Type III, displaying less intense interference colors, pronounced fibrous texture and a slightly opaque, mottled appearance.

mineral is typically present as colorless surface textures of massive habit inside the inner walls of cavities, identifiable under crossed polarizers due to its optical isotropy (Fig. 7a). The relative abundance of analcime is positively correlated with both temperature and the degree of palagonitization. The amount of analcime is found to generally have increased in samples from nearly all depths from 1979 to 2017.

5.2.3. Clay minerals

A variety of clay minerals, identified through XRPD (Grimaldi, 2018) as consisting of nontronite, montmorillonite and vermiculite, are present within all tuff samples investigated in this study. Granular to platy mineral aggregates displaying high interference colors are commonly found in available pore space. Clay minerals also occur in the form of alteration rims around olivine phenocrysts. Lastly, submicroscopic to microscopic clay minerals appear as replacement product of sideromelane in palagonitized glass. XRPD does not allow for discrimination between different clay mineral species at their distinct structural positions. The abovementioned highly birefringent dark brown cryptocrystalline clay mineral rims on olivine grains (Fig. 7b, c) are observed exclusively below water level. Above water level olivine typically appears unaltered under the microscope in both SE-01 and SE-02b. The thickness of the olivine alteration rims is positively correlated with temperature. The rims are not observed in samples from the poorly altered zones in the cores between ca. 138–150 m, as well as from the very bottom of both drill holes below 159 m in SE-01 and 178 m in SE-02b respectively.

5.2.4. Tobermorite

Tobermorite (general formula: $Ca_5Si_6O_{16}(OH)_2 \cdot 7H_2O$) is present as colorless acicular crystals, arranged as either discrete needles or sheaf like bundles (Jakobsson and Moore, 1986) (Fig. 7d). It commonly forms within cavities and is frequently associated with analcime as well as phillipsite in some samples, particularly below water level (Fig. 8b).

5.2.5. Phillipsite

In thin section phillipsite (general formula: $(K,Na,Ca)_{1-2}(Si,Al)_8O_{16} \cdot 6H_2O$) occurs as colorless intergrowing prismatic crystals often radiating from a common point of origin. Under crossed polarizers it is distinguishable by its low interference colors (gray I) (Fig. 7e). It commonly fills smaller (50–200 µm) pores and, unlike analcime, only rarely occurs as surface textures in larger cavities. Phillipsite concentrations in the tuff samples appear to have decreased in the higher temperature zones, most likely due to dissolution and/or replacement by other phases (Figs. 7f, 8). Samples that are particularly high in phillipsite are generally marked by a low degree of palagonitization and occasionally by the presence of type I palagonitized glass.

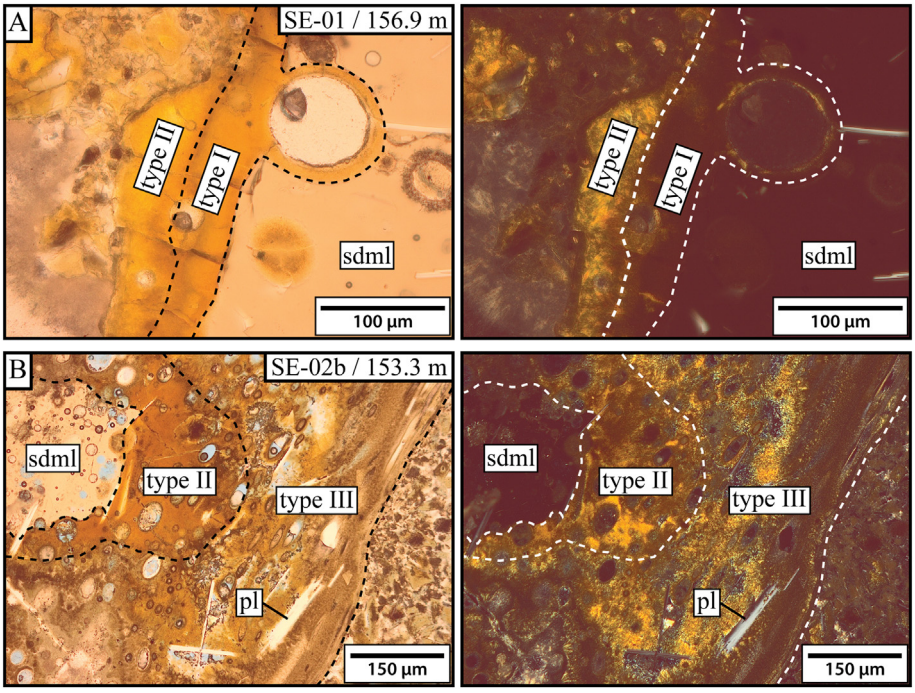

Fig. 6. Spatial relationships between the three different types of palagonitized glass textures. Where these occur together in the same lapillus, types I-III are typically concentrically arranged around sideromelane (i.e. seemingly "fresh" glass) in the sequence "type III → type II → type I → sideromelane" starting at the outer edge of the grain and moving towards the glass-palagonite interface. This observation is consistent with a model of progressive palagonite maturation, in which gel-palagonite, i.e. type I, is first formed along the glass-fluid interface, before undergoing a continuum of alteration processes over time and forming types II-III as the palagonitization front progresses inwards towards the core of fresh glass in the basaltic lapillus.

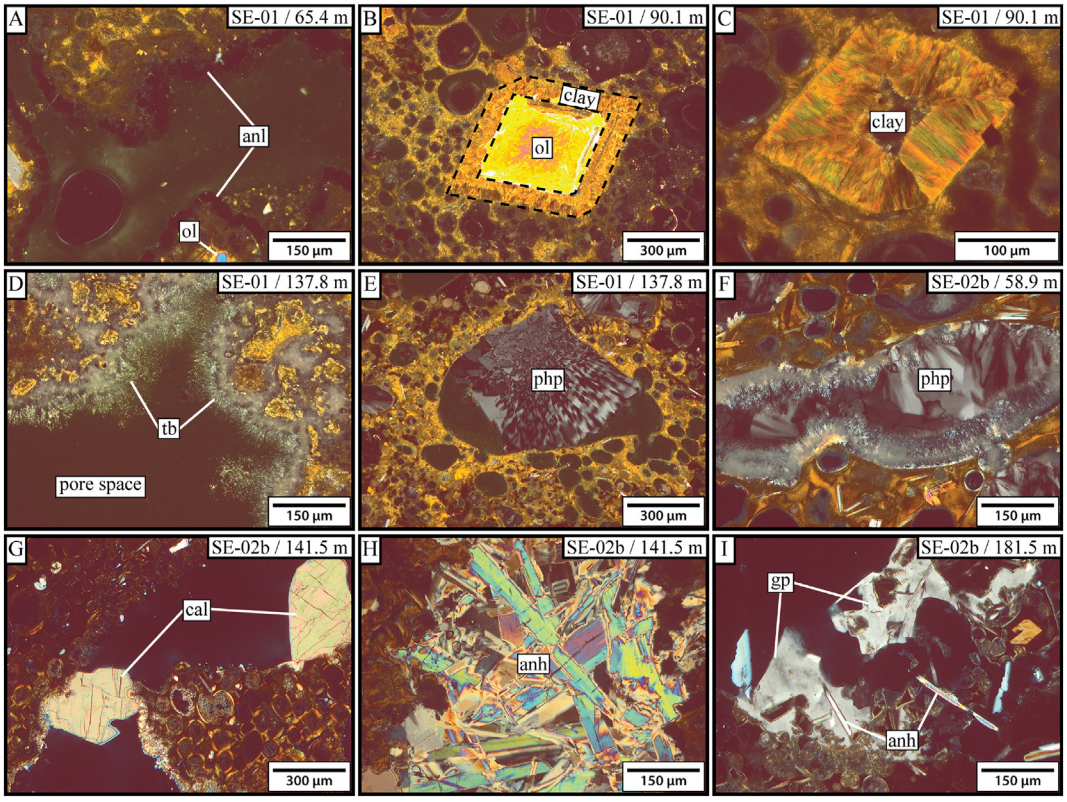

Fig. 7. Overview of the most common authigenic minerals in Surtsey tuff from the archived 1979 SE-01 drill core and the 2017 SE-02b drill core. A) Optically isotropic analcime surface textures in pores. B) Clay mineral alteration rim on an olivine single crystal. C) Nearly complete pseudomorphic alteration of olivine to clay minerals. D) Acicular tobermorite surface texture in a pore. E) Prismatic phillipsite in a vesicle. F) Precipitation of phillipsite in a pore with tobermorite surface texture and subsequent dissolution below water level. G) Massive calcite in the poorly altered zone. F) Prismatic intergrowths of anhydrite from the poorly altered zone. G) Gypsum and anhydrite near the base of the SE-02b drill hole. Mineral Abbreviations, where applicable, after Whitney and Evans (2010).

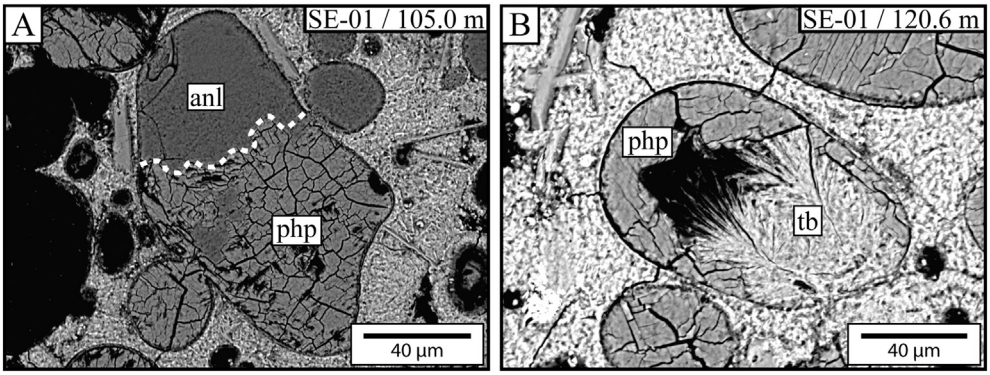

Fig. 8. Backscatter electron micrographs showing A) the partial alteration of analcime to analcime in a lapillus vesicle and B) the growth of tobermorite in a vesicle with phillipsite surface texture.

5.2.6. Calcite

Calcite occurs infrequently above and below water level. In more shallow depths, calcite is present as small (≤10 μm) massive to prismatic grains displaying characteristically high interference colors. Calcite crystals below water level are frequently larger than their counterparts above water level. In SE-02b between 140 and 150 m, several samples show particularly high calcite contents (Fig. 7g).

5.2.7. Calcium sulphate minerals

Anhydrite ($CaSO_4$) and gypsum ($CaSO_4 \cdot 2H_2O$) are generally present in trace amounts in most samples. Anhydrite occurs as granular to prismatic crystals ≤10 μm in size, which appear to have precipitated after tobermorite as a result of late stage hydrothermal alteration. Samples from the poorly altered portion of the cores between ~138 and 150 m and from the bottom of the drill holes contain larger prismatic or, more rarely, massive anhydrite crystals (Fig. 7h) in pore space or as fillings within fractures.

Only traces of gypsum were detected in the XRPD diffraction measurements of SE-01 samples. In SE-02b gypsum is observed under the microscope above water level at 31.2 m and 40.4 m as well as in the poorly altered zone at 144.1 m and near the bottom of the core around 180 m, where it can be found either by itself as massive, tabular or amygdaloidal crystals or together with prismatic anhydrite (Fig. 7i). XRPD diffraction also identified bassanite ($CaSO_4 \cdot 0.5H_2O$) in the sample from 169.5 m depth in SE-01.

5.3. Alteration in archived 1979 SE-01 drill core samples

5.3.1. Palagonitized glass

Above water level, the degree of palagonitization is between 73.3 and 82.4 vol%, except for the sample from 43.6 m, which is only 21.6 vol% palagonitized. The most common type of palagonitized glass at these depths is the optically isotropic, presumably amorphous type I, or gel-palagonite. All samples above 65.4 m depth are relatively high in X-ray amorphous contents (generally around 60–70 wt%). At 55.8 m, palagonitized glass rim thickness, as well as palagonitization extent begins to rapidly increase with depth. Despite the degree of palagonitization being 95.5–100.0 vol% at almost all depths from 65.4–120.6 m, a poorly palagonitized layer exists around 95.4 m, in which nearly half of the sideromelane remains unaltered. This layer is darker and finer grained compared to surrounding tuff and exhibits very low porosities. It forms a sharp border with the underlying tuff at 95.5 m, which exhibits higher porosity and a very high degree of palagonitization of >95.0 vol% (Table 1). Between 55.8–105.0 m, 120.6–137.8 m and 150.3–156.9 m, type II palagonitized glass (fibropalagonite) is generally the most abundant form of palagonitized glass. The amount of X-ray amorphous contents for these samples is normally below 60 wt% – except for the two samples from 55.8 to 65.4 m (Grimaldi, 2018). Only the three samples retrieved from 105.0 m, 111.0 m and 120.6 m, the first two of which correspond to the zone of maximum temperature, contain type III palagonitized glass. X-ray amorphous contents are highest at 105.0 m, at 85 wt%. Samples from the depth interval between 137.8 and 150.3 m generally show either very little palagonitization or the glass appears entirely unaltered under the petrographic microscope. The amount of X-ray amorphous phases for these samples is 68–70 wt%. Only type I rims with a median diameter of 40 μm are present at 148.3 m. The sharp lower boundary of this interval is visible at the macro- and microscopic scales. The rock turns from a grayish, friable, poorly consolidated and mostly unpalagonitized lapilli-tuff to a more well consolidated, slightly palagonitized lapilli-tuff that contains thin type II palagonitized glass rims, ranging between 20 and 90 μm. This change is not gradual but abrupt, occurring over just a few μm in the thin section of the sample from 150.3 m. The transition is accompanied by a decrease in the X-ray amorphous content from 68 wt% in the unpalagonitized upper half of this sample to 59 wt% in the slightly palagonitized lower half. The degree of palagonitization slightly increases with depth between 150.3 and 156.9 m. Below 156.9 m no palagonitized glass rims are detected under the microscope. However, nano-analytical techniques may reveal minor alteration features on a submicroscopic scale at these depths (Jackson et al., 2019b).

5.3.2. Clay minerals

Clay minerals are found throughout most of the samples in SE-01, as microcrystalline highly birefringent granular to platy mineral aggregates in pore space and as microscopic to submicroscopic granular particles in palagonitized glass. At 72.4 m clay minerals also begin to appear as rims on olivine grains as a pseudomorphic alteration phase (Fig. 7b). The thickness of these rims ranges from 20 to 95 μm and varies as a function of temperature. In some instances, olivine has become entirely replaced by secondary clay minerals (Fig. 7c). Olivine rims are not observed under the microscope in samples from the interval between 140.0 and 150.3 m. Below this depth interval only 20 μm thin rims are observed in the sample from 156.9 m.

5.3.3. Phillipsite

Phillipsite contents are higher than analcime in some samples above water level (Table 1, Fig. 9). Particularly high amounts of phillipsite are found in the tuff at 22.0 m, which contains 5.5 vol% (point counts)/11 wt % (XRPD) of this mineral, as opposed to only about 4.1 vol%/7 wt% analcime. Below water level, the amount of phillipsite begins to decrease with depth and remains generally low above 137.8 m. Several phillipsite grains show signs of dissolution and replacement by analcime and tobermorite (Fig. 8). The samples from 137.8 m, 148.3 m and 150.3 m are enriched in phillipsite compared to other samples below water level. These samples contain significantly more phillipsite than analcime, which is unusual below water level.

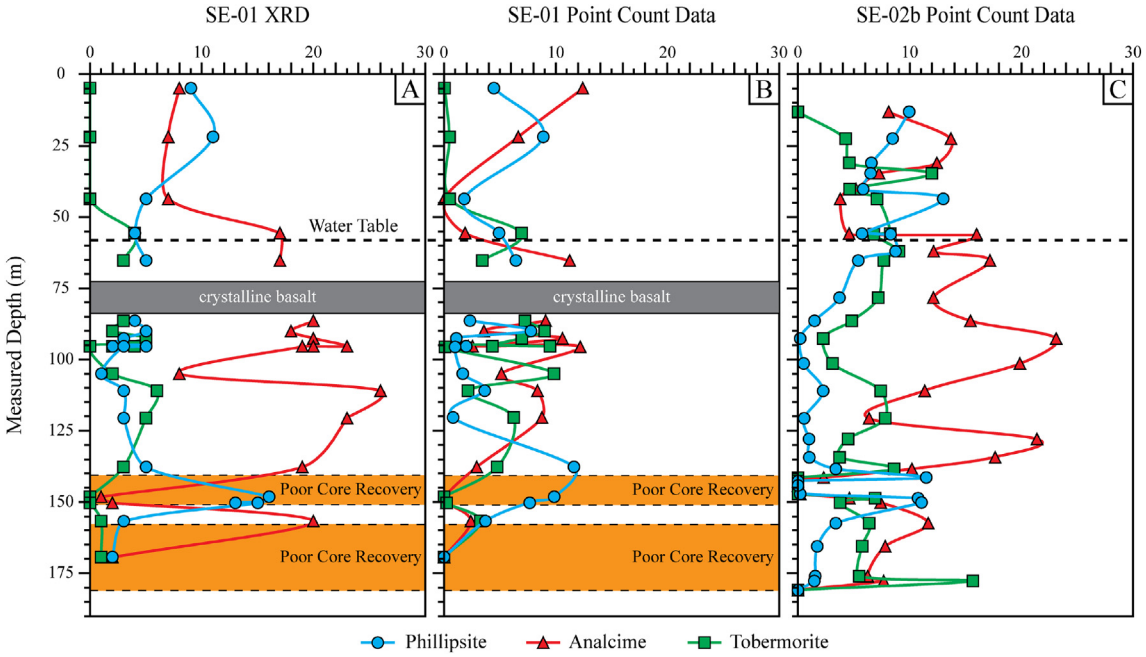

Fig. 9. Relative distributions of phillipsite, analcime and tobermorite in the Surtsey drill cores based on A) x-ray diffraction (wt%) and B) & C) point counts (vol%). The point count data is provided as pore space free. Overall, analcime content has increased at nearly all depths. Phillipsite content has increased only in certain samples above 65.4 m depth and in parts of the poorly altered zone. SE-02b contains slightly less phillipsite than SE-01 in the depth interval between 65.4 and 138.4 m. The top and bottom of the poorly altered zones situated between about 138–150 m show increases in phillipsite, but no increase in analcime and tobermorite. Tobermorite has mostly increased above water level and towards the bottom of the drill hole, but has decreased overall in the area of maximum temperature. Due to incomplete core recovery in SE-01 only cutting samples were available at some depth intervals within the poorly altered zone and towards the bottom of the drill core. For more information on the exact depths, refer to Table 1.

5.3.4. Analcime

Analcime shows a positive correlation with both degree of palagonitization and temperature. Its contents strongly increase below water level and reach peak amounts of up to 26 wt% according to XRPD between 95.5 and 111.0 m, which roughly coincides with the area of maximum temperature in the system. The top and bottom borders of the poorly altered and very friable interval spanning the area below 137.8 m, down to 150.3 m contain very little to no analcime and are instead dominated by phillipsite (see above). Much like phillipsite and tobermorite, analcime is not observed in any relevant quantities below 157.3 m depths, where consolidation of the tuff and the degree of palagonitization remain exceedingly low.

5.3.5. Tobermorite

Thin section petrography and XRPD identified very little to no (typically <1 wt%/vol%) tobermorite in SE-01 above water level. Below water level tobermorite is weakly correlated with temperature and the degree of palagonitization. Similar to analcime, tobermorite reaches its maximum concentrations in the samples around the area of highest temperature between 95.4 and 111.0 m, with the exception of a narrow zone around 95.6 m where the rock is intersected by a series of discrete fractures filled with calcium sulphate mineral phases, identified as anhydrite in thin section, as well as possibly minor amounts of gypsum according to XRPD. This specific sample contains virtually no tobermorite, despite originating from the general area of highest tobermorite concentrations. Tobermorite is only detected in traces via XRPD in the seemingly unpalagonitized sample from 169.5 m and not observed at all in the corresponding thin section.

5.3.6. Calcium sulphate minerals

Calcium sulphates occur throughout the samples from SE-01. Many samples, especially above water level, contain small (≤10 μm) prismatic to granular anhydrite often associated with tobermorite. Enrichment in anhydrite, resulting in the formation of larger prismatic crystals of ca. 200–700 μm length, occurs in several samples below water level. Examples for this include the lower contact between the basaltic intrusion and the tuff at 83.5 m, 95.6 m, where anhydrite occurs as filling in fractures, 105.0 m, 150.3 m, and especially 169.5 m, where anhydrite is strongly enriched in the otherwise seemingly unaltered vitric tuff of this depth.

While anhydrite is the only calcium sulphate phase identified in thin section, XRPD also detects gypsum and bassanite. Gypsum occurs mostly in traces in several samples throughout the core and potentially in larger quantities below the basaltic intrusion at 83.5 m, though this is not observed in the thin section sample. Bassanite is detected only at 169.5 m, with increased anhydrite content.

5.3.7. Calcite

Minor amounts of massive to prismatic calcite are scattered throughout the tuff of the 1979 core. Individual crystals are typically ≤10 μm in diameter and appear to have formed after analcime and tobermorite above water level and before or simultaneous with analcime below water level. No particular patterns or enrichments for this mineral are observed in SE-01.

5.4. Alteration in 2017 SE-02b drill core samples

5.4.1. Palagonitized glass

Samples from the uppermost section of the system situated above the tidally influenced water level, are not fully palagonitized. Rather, the degree of palagonitization remains relatively steady between 22.6 and 56.0 m at around 82.0 vol% (Table 1, Fig. 4). Type I palagonitic textures are prevalent in this part of the system but have locally been replaced by the more crystalline and highly birefringent type II rims at 31.2 m and below. The degree of palagonitization is ≥90.0 vol% for all samples between water level and 141.5 m. The tuff between 141.5 m and 147.1 m remains only weakly palagonitized. Type III palagonitic textures are far more widespread below water level than in SE-01 and

dominate in samples between 67.5 and 134.3 m. SE-02b samples corresponding in depth to the weakly altered and poorly consolidated interval between 157.5 and 177.8 m in SE-01 are nearly completely palagonitized. A concentric arrangement of palagonitized glass rims in the form type III → type II → type I → sideromelane is very common below 150.3 m.

5.4.2. Clay minerals

The distribution of clay minerals in SE-02b is the same as in SE-01. Both granular to platy aggregates in pore space and microscopic to submicroscopic particles in palagonitized glass are common. In SE-02b the first signs of olivine alteration to clay minerals are detected at 62.1 m, slightly below the water table in the borehole (~58 m, Weisenberger et al., 2019). Olivine alteration rims show greater diameters in samples from SE-02b, when compared to depth-equivalent samples from SE-01 (Fig. 4). No alteration rims are observed along olivine grains within samples between 141.5 and 150.3 m or in the bottom section of the drill core below 177.8 m where no palagonitization has been detected from our petrographic analysis. However, thin olivine rims about 20–45 μm in thickness are generally found between these depth intervals at 157.5–177.8 m.

5.4.3. Phillipsite

Samples from the uppermost 62.1 m of SE-02b contain more phillipsite than samples at corresponding depths in SE-01. The greatest enrichment of phillipsite in SE-02b is found around 43.7 m, where the tuff remains slightly altered and only poorly palagonitized in SE-01, but the overall extent of alteration is much greater in SE-02b. Consistently lower amounts of phillipsite are present from 65.4 to 138.4 m in SE-02b as compared to SE-01 (Table 1, Fig. 9). Phillipsite dissolution and replacement by analcime and tobermorite is observed throughout most of the samples, even at depths where phillipsite has increased since 1979. The phillipsite-rich upper and lower borders of the poorly altered depth interval, located in SE-01 between 137.8 and 150.3 m show increased phillipsite contents in SE-02b as well, although the upper zone of enrichment is found at a slightly greater depth at 141.5 m in the 2017 core. The lower phillipsite enriched zone is found at 150.3 m, at the same measured depth where it was detected in SE-01.

5.4.4. Analcime

Similar to SE-01, analcime contents are positively correlated with temperature and the degree of palagonitization in SE-02b. The amount of analcime has increased from 1979 to 2017 at almost all depths and is highest at 92.6–101.5 m, where it has about doubled. As is the case with phillipsite and tobermorite, secondary analcime mineralization has extended into previously weakly altered tuff between 157.5 and 177.8 m.

5.4.5. Tobermorite

Point counts of thin sections at 43.6 m and above indicate significantly higher tobermorite content than their SE-01 counterparts, which contain almost no tobermorite (Table 1). In these samples, tobermorite is frequently associated with other Ca-bearing phases such as plagioclase, clay minerals or gypsum. Particularly the sample at 34.8 m containing 9.3 vol% tobermorite exhibits some of the highest concentrations of this mineral observed in any of the studied samples from either drill core. In the hottest areas of the system tobermorite contents are found to be lower in SE-02b than in SE-01, with the samples between 86.5 and 101.5 m all showing less tobermorite than the samples from SE-01 from comparable depths. Two distinct peaks in tobermorite content are found in the samples at 138.4 and 148.7 m, at depths where previously only phillipsite had been enriched, but little to no increase in tobermorite or analcime content was detected in the 1979 samples. The highest concentrations of tobermorite of 14.3 vol% are present in the sample from 177.8 m, which is situated close to the very bottom of the palagonitized area in SE-02b.

5.4.6. Calcium sulphate minerals

The poorly altered zone contains high quantities of calcium sulphate phases. Gypsum, which in SE-01 is only identified via XRPD, but not observed in thin section, is abundant and observable under the microscope in SE-02b at 144.1 m. It typically either occurs alone or around prismatic anhydrite, with which it is frequently associated. Larger gypsum crystals are also found at 31.2 m and 40.4 m in the meteoric part of the system. In these samples gypsum seems to become partially replaced by tobermorite. Anhydrite and gypsum are the most common alteration minerals below 177.8 m, where no palagonitization is observed under the microscope in the 2017 drill core.

5.4.7. Calcite

Calcite is primarily found in larger amounts together with gypsum and anhydrite between 141.5 and 150.3 m. There, it forms massive, up to 400 μm large crystals (Fig. 7g) filling smaller vesicles or growing on the inside of larger fractures. Smaller amounts of calcite are especially found above water level, where all samples contain at least some traces of this mineral. Very little to no calcite occurs in the bottom part of the hole, where gypsum and anhydrite, the phases it is otherwise often associated with, are very common.

5.5. Alteration sequence and changes in secondary mineralogy

Two authigenic zeolite species, phillipsite and analcime, have been identified. Chabazite as described by Jakobsson and Moore (1986) for the upper 0–4 m of the SE-01 drill core, is not reported here, most likely owing to the fact that the most shallow samples in this study were from 4.9 m and 13.2 m for SE-01 and SE-02b respectively, which is below the documented depth range for this zeolite phase. Analcime is positively correlated with temperature and the degree of palagonitization. Phillipsite is more abundant in samples that show a lower extent of glass alteration overall, and comparatively lower amounts of analcime and tobermorite. Examples include the samples from 22.0, 137.8, 148.3 and 150.3 m depths in SE-01 and from 43.7, 141.5 and 150.3 m depths in SE-02b (Table 1, Fig. 9). Point count data confirms a net loss of phillipsite at 65.4–138.4 m between 1979 and 2017. Thin section petrography indicates that this may be due to dissolution of phillipsite as well as alteration to other phases, such as analcime. Thus, phillipsite may form as an earlier alteration product when compared to analcime both above and below the water table and become lost – at least below water level – due to dissolution as glass alteration progresses and the compositions of interstitial fluids change. The amount of phillipsite has either remained the same or increased in samples below approximately 150 m, where little alteration was observed in SE-01. Increased alteration rates of palagonitized glass and olivine rims are estimated for the SE-02b drill core samples at this depth interval (see Section 6.3.1 Alteration rates in zone 4). Tobermorite overgrows analcime or occurs alongside of it on the inner walls of pores and fractures. In contrast, analcime is rarely found overgrowing tobermorite. While gypsum is only detected via XRPD and not observed in thin section for the SE-01 sample set, several thin section samples from SE-02b – particularly between 142.6 and 147.1 m and below 177.8 m – are found to contain gypsum. Gypsum is therefore interpreted as having formed relatively late, as opposed to anhydrite which is already present in relevant quantities in the 1979 samples (Table 1).

6. Discussion

6.1. Time-lapse alteration with depth

Tephra alteration in Surtsey's hydrothermal system changes as a function of time and depth. We identify five zones of distinct alteration behavior observable in both the 1979 and 2017 drill cores. An overview

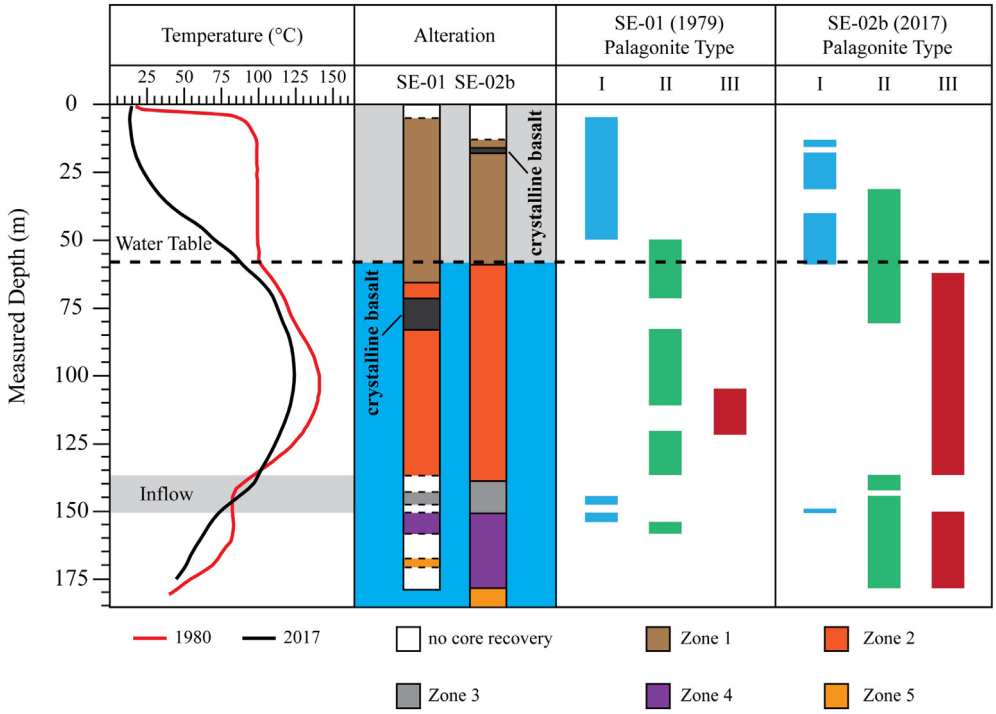

Fig. 10. Integrated log displaying the relationship between temperature, alteration progress and maturation of palagonitized glass determined through petrographic investigations of thin sections in the archived 1979 SE-01 drill core and the 2017 SE-02b drill core.

of the zones and associated changes in alteration behavior is given in Fig. 10. The alteration zones are defined as follows:

6.1.1. Zone 1 (upper palagonitization zone)

In zone 1, situated above 65.4 m in SE-01 and 58.9 m in SE-02b, palagonitization progresses slowly, when compared to the remaining palagonitized parts of the system. No olivine alteration is observed. Phillipsite contents are locally higher than analcime contents, especially in less palagonitized samples, and have either increased or remained steady between 1979 and 2017. Zone 1 persists slightly below water level, which lies around 58 m depth.

6.1.2. Zone 2 (middle palagonitization zone)

Below zone 1, secondary clay mineral rims begin to form around individual olivine grains, eventually leading to complete pseudomorphic replacement. The onset of this alteration marks the beginning of zone 2, reaching down from the bottom border of zone 1 to 137.8 m in SE-01 and 138.4 m in SE-02b. At the transition between zones 1 and 2 palagonitization rim thicknesses suddenly increase by two to four times, resulting in a strong increase in the degree of palagonitization (Fig. 4). This increase is observed in both cores. The most common type of palagonitic rim in zone 2 is type II in SE-01, which has evolved to type III in SE-02b, reflecting a more rapid palagonite maturation in zone 2 as compared to zone 1. Alteration degree and thus rim thicknesses for both palagonitized glass and olivine rims increase steadily as a function of temperature.

The amount of analcime present in the tuff is positively correlated with the degree of palagonitization and temperature. In contrast, phillipsite in zone 2 noticeably decreases between 1979 and 2017. Petrographic observations suggest, that the reason for this lies mainly in the dissolution of phillipsite, with simultaneous replacement by analcime and tobermorite. This may be partially due to the higher amounts of Na^+ present in the system below sea level, which may favor the formation of analcime over phillipsite. Additionally, zeolite distribution in hydrothermally altered rocks is also known to be governed to a large extent by temperature (Browne, 1978; Kusakabe et al., 1981; de Gennaro et al., 1999; Langella et al., 2001; Kralj, 2016). For this reason, the local dominance of phillipsite over analcime in more shallow depths may also be caused by the relatively lower temperatures, as phillipsite would be expected to be more stable under colder conditions, when compared to analcime (Chipera and Apps, 2001). Host-rock lithology may influence the type of zeolite being precipitated under low-temperature hydrothermal conditions (Browne, 1978; Reyes, 2000), such as the ones present in the Surtsey hydrothermal system, but this is unlikely to contribute in any significant way, as the Surtsey system is almost entirely hosted in universally poorly sorted intermediate to coarse alkali basaltic lapilli-tuff, showing only minor chemical or lithological variation (Schipper et al., 2015). As phillipsite appears to be an early stage alteration product, the comparatively higher phillipsite contents within zone 1 may also be due to the lower degree of palagonitization and therefore less advanced reaction progress.

In SE-01, zone 2 hosts a thin ash-rich layer of darker material that is noticeably less porous and less palagonitized than the surrounding rocks at 95.4 m, which coincides with a reduction in secondary mineral content (Table 1). The low porosities and therefore low permeabilities in this layer likely inhibit hydrothermal circulation and locally counteract the precipitation of secondary minerals and devitrification of the glass at this depth. No ash-rich layer exhibiting similar properties is observed in SE-02b, implying that this feature is either transient in nature or highly localized.

6.1.3. Zone 3 (poorly altered zone)

Both cores contain a poorly altered zone that is partially unconsolidated in 1979 and lightly consolidated in 2017. It encompasses the depth interval from 137.8 to 150.3 m in SE-01, but has slightly shrunk in diameter in SE-02b, where it reaches between 138.4 and 150.3 m. The sideromelane of the poorly altered zone remains largely unpalagonitized. Only a few thin layers of slightly palagonitized tephra are observed. The lack of palagonitization and consolidation by mineral cements arguably led to the poor core recovery during the 1979 drilling expedition between 140.0–143.8 m and 148.5–150.3 m (see Jakobsson and Moore, 1982). In SE-02b zone 3 is slightly more consolidated, but the rocks remain highly porous and friable even in 2017. In both SE-01 and SE-02b, the upper and lower boundaries of zone 3 are marked

by a strong enrichment in phillipsite in otherwise weakly altered tuff. In SE-02b the upper phillipsite enriched interval has moved further down to 141.5 m (Table 1, Fig. 9). Phillipsite contents have decreased strongly in the now more extensively altered tuff between 137 and 138 m, while both tobermorite and analcime have increased in abundance. This is likely because phillipsite forms mainly in the initial stages of glass alteration before becoming replaced by other phases as the reaction progresses. Calcium sulphates such as anhydrite and gypsum are very common and particularly characteristic for zone 3.

An electrical resistivity log acquired after drilling of SE-02b (Jackson et al., 2019a; Weisenberger et al., 2019) indicates a change within the depth interval coinciding with zone 3. According to 16 s rRNA gene sequencing, roughly half of the prokaryotic community composition present in rock samples from SE-02b at 148 m depth, is shared with the one in seawater around the island (personal correspondence from Bergsten, 2019). However, it cannot be excluded that this is caused by seawater contamination during drilling. Here it is proposed, that zone 3 most likely marks an interval of high permeability and sea water recharge. This would further explain the presence of anhydrite and gypsum, as Ca^{2+} and SO_4^{2-} bearing fluids entering the system might precipitate a calcium sulphate phase upon being heated due to retrograde solubility.

6.1.4. Zone 4 (lower palagonitization zone)

Zone 4, between 150.3 and 157.3 m in SE-01 and 150.3–177.8 m in SE-02b, shows the greatest change since 1979. In SE-01 alteration behavior in zone 4 resembles that of zone 2, though overall alteration is less extensive. In SE-02b both palagonitization and olivine rim formation rates are much higher than predicted by the temperature-alteration-trends derived from samples in zones 1 and 2 (Fig. 11). The fact that this is not observed in samples from SE-01 indicates, that alteration in zone 4 has increased over time. The co-appearance of all three types of palagonitized glass rims, mostly II and III, arranged concentrically around sideromelane grains in the order type III → type II → type I → sideromelane is common in zone 4 in SE-02b (Fig. 6). As temperature is not the driving factor for the increase in alteration rates at this depth, other potential explanations may be found in chemical changes in the hydrothermal fluid or potentially in the water-rock ratio of the environment (Pauly et al., 2011).

6.1.5. Zone 5 (bottom zone)

The area below zone 4 in each core contains mostly fresh and apparently unaltered sideromelane. Absence of palagonitization and significant mineral cementation by zeolites and tobermorite in pore space causes the tephra of this zone to be largely unconsolidated. No olivine rims are detected under the microscope. Observed secondary mineralization is limited to mostly anhydrite and possibly bassanite in SE-01. In SE-02b both gypsum and anhydrite are observed.

6.2. Olivine alteration rates

Olivine alteration rates were estimated by dividing olivine rim thicknesses by time (assuming a 12-year timespan for SE-01 and a 50-year timespan for SE-02b) and plotting the results against temperature logging data from 1980 and 2018 to best approximate the current state of the system. Since temperature is related to alteration rates, these values should not be taken as fully accurate representation of the system's effective temperature, which varied over time. For samples from below 156.9 m, where no olivine rims are found in SE-01, a time period of 38 years for the alteration is assumed instead, as this value would be closer to the actual amount of time available for the alteration to progress. Our results confirm a positive relationship between olivine alteration rates and temperature, as first documented by Jakobsson and Moore (1986). The olivine alteration rates derived from the present study are slightly higher than those given by Jakobsson and Moore (1986), which is likely due to differences in methodology, specifically in the temperature values used. Regardless of the total extent of alteration rates, new insights are gained regarding the nature of the olivine-clay mineral reaction in the Surtsey tuff. Based on the analyses of the SE-01 core samples immediately after drilling and the temperature history of the system as of 1980, Jakobsson and Moore (1986) hypothesized a threshold temperature of 120 ± 5 °C for the alteration of olivine to clay minerals. They cited this as a potential reason for the absence of olivine rims above water level, as temperatures would not have exceeded 100 °C in that part of the system. However, our data from the 2017 drill core provide evidence that olivine rim formation can occur at lower temperatures within the hydrothermal system given enough time. In the SE-02b samples we observe 20–50 μm thick alteration

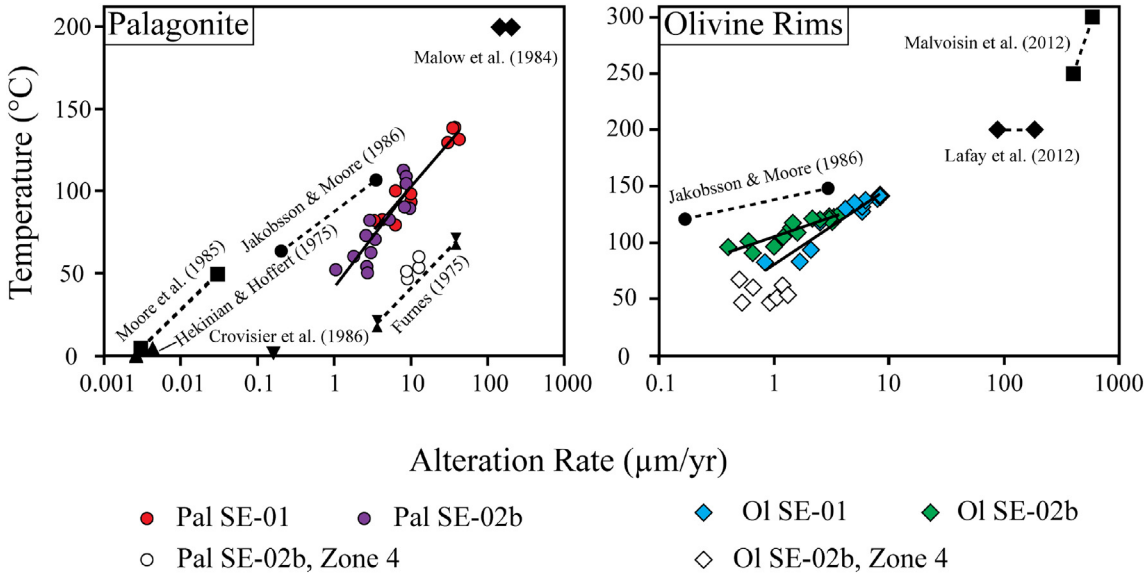

Fig. 11. Alteration rates inferred from the thicknesses of authigenic rims on palagonitized glass lapilli and olivine as a function of temperature for samples from the archived 1979 SE-01 and the SE-02b drill cores and comparison with results from other studies (Furnes, 1975; Hekinian and Hoffert, 1975; Malow et al., 1984; Moore et al., 1985; Jakobsson and Moore, 1986; Crovisier et al., 1986; Malvoisin et al., 2012; Lafay et al., 2012). While a trend for the alteration rates as a function of temperature can be reconciled for most depths, the samples retrieved from zone 4 show higher alteration rates than what would be predicted based on the trends established by samples from more shallow depths.

rims on olivine at 134.3–138.4 m and in zone 4 at 157.5–177.8 m. At these depths, temperatures have ranged from ca. 44–103 °C between 1980 and 2017 (Fig. 3), which is well below the threshold temperature proposed by Jakobsson and Moore (1986). Temperature alone can therefore not be the reaction's sole limiting parameter.

Lafay et al. (2012) performed autoclave experiments on olivine under alkaline conditions at 150–200 °C to study the rate of olivine replacement during serpentinization, measuring the fraction of grains <30 μm, 30–56 μm and 56–150 μm that remained after a given time interval. Their results and those of Malvoisin et al. (2012) are used to estimate alteration rates for serpentinization in $\mu m \cdot yr^{-1}$, which are plotted in Fig. 11 for comparison.

6.3. Palagonitization rates

Estimation of palagonitization rates was performed analogously to olivine alteration rates (see above). As samples from below 156.9 m remain unpalagonitized in 1979, a timespan of 38 years, between 1979 and 2017, is assumed as base for the alteration rates of these samples. It should be noted that Jackson et al., (2019b) identified minimal glass alteration at this depth by using X-ray microdiffraction. Palagonitization rates for samples from either drill core are correlated positively with temperature and generally plot along two highly similar trendlines (Fig. 11). In their 1986 study of SE-01, Jakobsson and Moore reported palagonitization rates of ca. 0.2–3.5 $\mu m \cdot yr^{-1}$ for alteration rims in glass lapilli. This contrasts with our results, which range between 3.33 and 42.50 $\mu m \cdot yr^{-1}$ for samples from the same drill core. It is likely that the reason for this discrepancy and that of the olivine alteration rates lies in a difference in the approach used. For instance, no universal stage was employed in this study to measure the exact angle of the rims. Our results nevertheless reproduce the same general trends in terms of palagonitized rim thickness variations with depth. In addition, Jakobsson and Moore (1986) estimated the effective temperature based on several parameters, whereas in this study a direct measurement is used. These factors are thought to contribute to the deviations between the two studies.

Palagonitization rates of comparable magnitude to those in our study have been achieved in experiments conducted by Furnes (1975) at temperatures comparable to those prevalent in Surtsey's hydrothermal system. Thomassin (1984) demonstrated experimentally that a palagonitic rim "several micrometers in thickness" can be formed in as little as nine months for samples heated in seawater using a Teflon reactor. Malow et al. (1984) derived even higher alteration rates for samples leached in NaCl solutions heated to 200 °C. Our results, though different from those of Jakobsson and Moore (1986), are therefore still within established parameters.

6.3.1. Alteration rates in zone 4

Palagonitic and olivine alteration rims indicate much higher alteration rates in the tuff from 150.3–177.8 m than predicted based on temperature alone (Fig. 11). Many of these rocks remained largely unaltered in 1979, meaning that the visible onset of palagonitization and olivine alteration would have commenced at an unspecified time after 1979, but before 2017. From this it can be concluded that the true alteration rates at this depth may be even higher than estimated here, since the alteration would have occurred over a shorter time span than the assumed 38 years between 1979 and 2017. Even if palagonitization and olivine rim formation have been ongoing in these areas throughout the entire 50-year history of the hydrothermal system, alteration rates are still substantially higher than predicted by the temperature-alteration-rate trends established by more shallow depth intervals. Possible reasons for this may lie in evolving fluid compositions, such as changing salinities, or in a different water-rock ratio.

6.4. Palagonite maturation

Three different types of palagonitization are identified in the Surtsey tuff samples, which are distinct in their textural and optical properties. These type I-II-III palagonitized glass rims exhibit a progressively more granular to fibrous texture and less gel-like appearance. Peacock (1926) first recognized two texturally distinct types of palagonite – the amorphous gel-palagonite and the slightly crystalline "fibro-palagonite" – in his comprehensive review of the petrology of Icelandic tuffs. Stroncik and Schmincke (2001) recognized that after the initial palagonitization process the altered glass undergoes a series of aging steps over time. They state that crystallinity gradually increases as palagonite ages, ultimately resulting in the complete crystallization of the material to smectite and other authigenic minerals, a finding also confirmed by other workers (Singer, 1974; Berkgaut et al., 1994; Crovisier et al., 2003; Drief and Schiffman, 2004). The classification scheme proposed by Stroncik and Schmincke (2001) uses the ratio of amorphous to crystalline material in the altered glass to delineate between the initial gel-palagonite (aging step I, mostly amorphous), fibro-palagonite (aging step II, mostly crystalline), and fully crystalline smectite. In their study of the palagonitic alteration of hyaloclastites from Hawaii, Walton and Schiffman (2003) recognized the formation of a complex of minerals, intergrown at the nanometer scale and dominantly composed of smectite, which they called 'reddened smectite grain replacement' (Walton and Schiffman, 2003). This material can be considered analogous to fibro-palagonite as described by Peacock (1926) (Drief and Schiffman, 2004). Despite these differences in the applied classification scheme or nomenclature, these authors and many others have generally agreed that the increasing crystallinity of palagonitized glass develops as the result of palagonitic maturation over time by means of reaction towards equilibrium with the interfacing hydrothermal fluid; only the amorphous gel-palagonite likely representing the initial alteration product of sideromelane (Singer, 1974; Zhou et al., 1992; Stroncik and Schmincke, 2001; Crovisier et al., 2003; Drief and Schiffman, 2004; Pauly et al., 2011).

Based on this large body of prior observations, we interpret the different types of palagonitic textures in the Surtsey samples as indicative of progressive maturation. Type I palagonitization (or gel-palagonite) marks an early stage, with type II and III representing progressively more advanced stages, wherein crystallinity increases and the palagonitized glass takes on a fibrous texture, before turning an earthy, mottled and opaque shade of brown as the devitrification process advances (Fig. 5). The distribution of these three palagonitic types is correlated with temperature, with type I found mainly in the areas of lowest temperature – especially above water level – and type III found in the areas of highest temperature. An exception to this is the depth interval of rapid palagonitization in SE-02b between 150.3 and 177.8 m (zone 4; see above) (Fig. 10), where temperatures are low, but very little type I palagonitized glass is observed. Within the framework of this interpretation, type III palagonitic rims represent a highly advanced stage of the devitrification process, so that the term "palagonite" in the strict sense may not be fully applicable. The very high concentration of X-ray amorphous phases in SE-01 around the system's area of maximum temperature (Grimaldi, 2018), where type III is observed, potentially indicates that a large portion of the material may have recrystallized as poorly ordered clays (Brindley, 1977).

7. Summary

The systematic petrographic comparison of two parallel vertical drill cores from the eastern tephra pile of the Surtur crater at Surtsey volcano, recovered in 1979 and 2017, provides new petrographic insights into time-lapse alteration within the island's basaltic low-temperature hydrothermal system, which will serve as the basis for future geochemical analyses.

1. Five discrete zones of distinct alteration style are recognized in the two studied Surtsey drill cores. These zones (Fig. 10), are defined by their discrete alteration mineralogy, development of secondary phases over time, as well as alteration of basaltic glass. Their vertical positions differ only slightly between the 1979 and 2017 drill cores.
2. Alteration in the form of palagonitization, zeolitization and tobermorite formation has progressed rapidly in most of the zones except for parts of the poorly altered zone 3 at 138.4–150.3 m depth, where alteration does not appear to have progressed to a significant degree from 1979 to 2017.
3. The rates of glass and olivine alteration, as measured by alteration rim thicknesses, generally reproduce the trends established by Jakobsson and Moore (1986). Both types of alteration increase with temperature in the SE-01 samples and in the SE-02b samples above zone 4 (Fig. 11). In zone 4 of SE-02b alteration rates diverge from this general trend, yielding higher than expected rates of production for both palagonitized glass and altered olivine rims.
4. Phillipsite appears to be an early stage alteration product, for which the relative abundance has decreased in all samples between 65.4 and 138.4 m depths since 1979. This is consistent with petrographic observations, which show phillipsite dissolution or alteration to analcime and tobermorite.
5. Surtsey tuff samples show three principal types of palagonitized glass textures, which indicate progressive stages in the reaction of sideromelane to smectite. The distribution of these three palagonitic types in SE-01 and SE-02b shows clear progress in the ongoing devitrification of the Surtsey tephra deposits between 1979 and 2017.

Declaration of competing interest

The authors declare that there are no conflicts of interest.

Acknowledgements

Funding for this project was provided by the International Continental Scientific Drilling Program (ICDP) through a grant to the SUSTAIN project; a grant of excellence from the Icelandic Research Fund, ICF-RANNÍS; the Bergen Research Foundation and K.G. Jebsen Centre for Deep Sea Research at the University of Bergen, Norway; the German Research Foundation; and DiSTAR, Federico II, University of Naples, Federico II, Italy. The University of Utah, USA, and the two Icelandic power companies Reykjavík Energy and Landsvirkjun contributed additional funds for drilling. The authors would like to express their gratitude to Barbara I. Kleine, Pauline Bergsten, Carolyn F. Gorny and James G. Moore for constructive feedback on the topics of fluid geochemistry, microbiology and volcanology. We thank two anonymous reviewers for their detailed and constructive comments and José Luis Macías for his editorial efforts and the editorial handling of the paper.

References

Berkgaut, V., Singer, A., Stahr, K., 1994. Palagonite reconsidered: paracrystalline illite-smectites from regoliths on basic pyroclastics. Clay Clay Miner. 42, 582–592.
Bish, D.L., Chipera, S.J., 1987. Problems and solutions in quantitative analysis of complex mixtures by X-ray powder diffraction. Adv. X-ray Anal. 31, 295–308.
Brindley, G.W., 1977. Aspects of order-disorder in clay minerals-a review. Clay Sci. 5, 103–112.
Browne, P.R.L., 1978. Hydrothermal alteration in active geothermal fields. Annu. Rev. Earth Planet. Sci. 6, 229–248.
Chipera, S.J., Apps, J.A., 2001. Geochemical stability of natural zeolites. In: Bish, D.L., Ming, D.W. (Eds.), Natural Zeolites: Occurrence, Properties, Applications, pp. 117–157.
Crovisier, J.L., Eberhart, J.P., Honnorez, J., 1986. Dissolution of basaltic glass in seawater: mechanism and rate. Extended Abstracts of the Fifth International Symposium on Water-Rock Interaction. International Association of Geochemistry and Cosmochemistry, Reykjavik, Iceland, pp. 142–145.
Crovisier, J.L., Advocat, T., Dussossoy, J.L., 2003. Nature and role of natural alteration gels formed on the surface of ancient volcanic glasses (Natural analogs of waste containment glasses). J. Nucl. Mater. 321, 91–109.
de Gennaro, M., Langella, A., Cappelletti, P., Colella, C., 1999. Hydrothermal conversion of trachytic glass to zeolite. 3. Monocationic model glasses. Clay Clay Miner. 47, 348–357.
Drief, A., Schiffman, P., 2004. Very low-temperature alteration of sideromelane in hyaloclastites and hyalotuffs from Kilauea and Mauna Kea volcanoes: implications for the mechanism of palagonite formation. Clay Clay Miner. 52, 623–635.
Fisher, R.V., Schmincke, H.U., 1984. Submarine volcaniclastic rocks. Pyroclastic Rocks. Springer, Berlin, Heidelberg, pp. 265–296.
Friedman, J.D., Williams, R.S., 1970. Changing patterns of thermal emission from Surtsey, Iceland, between 1966 and 1969. US Geol. Surv. Prof. Pap. 700-D, pp. 116–124.
Frolova, Y.V., 2010. Patterns of transformations in the compositions and properties of icelandic hyaloclastites during lithogenesis. Mosc. Univ. Geol. Bull. 65, 104–114.
Furnes, H., 1975. Experimental palagonitization of basaltic glasses of varied composition. Contrib. to Mineral. Petrol. 50, 105–113.
Gernon, T.M., Hincks, T.K., Tyrrell, T., Rohling, E.J., Palmer, M.R., 2016. Snowball Earth ocean chemistry driven by extensive ridge volcanism during Rodinia breakup. Nat. Geosci. 9, 242.
Giggenbach, W.F., 1984. Mass transfer in hydrothermal alteration systems—a conceptual approach. Geochim. Cosmochim. Acta 48, 2693–2711.
Grimaldi, C., 2018. Quantitative Characterization of Zeolites From Surtsey Island (Iceland). (M.Sc. thesis). Department of Earth, Environmental and Resources Sciences at the University of Napoli Federico II, Italy.
Hekinian, R., Hoffert, M., 1975. Rate of palagonitization and manganese coating on basaltic rocks from the rift valley in the Atlantic Ocean near 36°50′N. Mar. Geol. 19, 91–109.
Henley, R.W., Truesdell, A.H., Barton, P.B., Whitney, J.A., 1985. Fluid-Mineral Equilibria in Hydrothermal Systems. Society of Economic Geologists.
Honnorez, J., 1978. Generation of phillipsites by palagonitization of basaltic glass in sea water and the origin of K-rich deep-sea sediments. In: Sand, L.B., Mumpton, F.A. (Eds.), Natural Zeolites: Occurrence, Properties, Use, pp. 245–258.
Jackson, M.D., Gudmundsson, M.T., Bach, W., Cappelletti, P., Coleman, N.J., Ivarsson, M., Jónasson, K., Jørgensen, S.L., Marteinsson, V.b., McPhie, J., Moore, J.G., Nielson, D., Rhodes, J.M., Rispoli, C., Schiffman, P., Stefánsson, A., Türke, A., Vanorio, T., Weisenberger, T.B., White, J.D.L., Zierenberg, R., Zimanowski, B., 2015. Time-lapse characterization of hydrothermal seawater and microbial interactions with basaltic tephra at Surtsey Volcano. Sci. Drill. 20, 51–58.
Jackson, M.D., Gudmundsson, M.T., Weisenberger, T.B., Rhodes, J.M., Stefánsson, A., Kleine, B.I., Lippert, P.C., Marquardt, J.M., Reynolds, H.I., Kück, J., Marteinsson, V.Þ., Vannier, P., Bach, W., Barich, A., Bergsten, P., Bryce, J.G., Cappelletti, P., Couper, S., Fahnestock, M.F., Gorny, C.F., Grimaldi, C., Groh, M., Guðmundsson, Á., Gunnlaugsson, Á.Þ., Hamelin, C., Högnadóttir, Þ., Jónasson, K., Jónsson, S.S., Jørgensen, S.L., Klonowski, A.M., Marshall, B., Massey, E., McPhie, J., Moore, J.G., Ólafsson, E.S., Onstad, S.L., Perez, V., Prause, S., Snorasson, S.P., Türke, A., White, J.D.L., Zimanowski, B., 2019a. SUSTAIN drilling at Surtsey volcano, Iceland, tracks hydrothermal and microbiological interactions in basalt 50 years after eruption. Sci. Drill. 25, 35–46.
Jackson, M.D., Couper, S., Stan, C.V., Ivarsson, M., Czabaj, M.W., Tamura, N., Parkinson, D., Miyagi, L.M., Moore, J.G., 2019b. Authigenic mineral textures in submarine 1979 basalt drill core, Surtsey volcano, Iceland. Geochemistry, Geophys., Geosystems 20, 3751–3773.
Jakobsson, S.P., 1971. Palagonitiseringen af tefraen på Surtsey. Natturufraedistofnun Islands, pp. 61–62.
Jakobsson, S.P., 1972. On the consolidation and Palagonitization on the Tephra of the Surtsey Volcanic Island, Iceland. Surtsey Res. Prog. Rep, pp. 121–128.
Jakobsson, S.P., 1978. Environmental factors controlling the palagonitization of the Surtsey tephra, Iceland. Bull. Geol. Soc. Denmark 27, 91–105.
Jakobsson, S.P., Moore, J.G., 1982. The Surtsey research drilling project of 1979. Surtsey Res 9, 76–93.
Jakobsson, S.P., Moore, J.G., 1986. Hydrothermal minerals and alteration rates at Surtsey volcano, Iceland. Geol. Soc. Am. Bull. 97, 648–659.
Jakobsson, S.P., Gudmundsson, G., Moore, J.G., 2000. Geological monitoring of Surtsey, Iceland, 1967–1998. Surtsey Res. 11, 99–108.
Kousehlar, M., Weisenberger, T.B., Tutti, F., Mirnejad, H., 2012. Fluid control on low-temperature mineral formation in volcanic rocks of Kahrizak, Iran. Geofluids 12, 295–311.
Kralj, P., 2016. Hydrothermal zeolitisation controlled by host-rock lithofacies in the Periadriatic (Oligocene) Smrekovec submarine composite stratovolcano, Slovenia. J. Volcanol. Geotherm. Res. 317, 53–65.
Kusakabe, H., Minato, H., Utada, M., Yamanaka, T., 1981. Phase relations of clinoptilolite, mordenite, analcime and albite with increasing pH, sodium ion concentration and temperature. Sci. Pap. Coll. Gen. Educ. Univ. Tokyo 31, 39–59.
Lafay, R., Montes-Hernandez, G., Janots, E., Chiriac, R., Findling, N., Toche, F., 2012. Mineral replacement rate of olivine by chrysotile and brucite under high alkaline conditions. J. Cryst. Growth 347, 62–72.
Langella, A., Cappelletti, P., de Gennaro, R., 2001. Zeolites in closed hydrologic systems. Rev. Mineral. Geochemistry 45, 235–260.
Lorenz, V., 1974. Studies of the Surtsey tephra deposits. Surtsey Res. Prog. Rep. 7, 72–79.
Malow, G., Lutze, W., Ewing, R.C., 1984. Alteration effects and leach rates of basaltic glasses: implications for the long-term stability of nuclear waste form borosilicate glasses. J. Non-Cryst. Solids 67, 305–321.
Malvoisin, B., Brunet, F., Carlut, J., Rouméjon, S., Cannat, M., 2012. Serpentinization of oceanic peridotites: 2. Kinetics and processes of San Carlos olivine hydrothermal alteration. J. Geophys. Res. Solid Earth 117.
Marshall, R.R., 1961. Devitrification of natural glass. Geol. Soc. Am. Bull. 72, 1493–1520.
Moore, J.G., 1966. Rate of palagonitization of submarine basalt adjacent to Hawaii. US Geol. Surv. Prof. Pap. 550, D163–D171.
Moore, J.G., 1985. Structure and eruptive mechanisms at Surtsey Volcano, Iceland. Geol. Mag. 122, 649–661.

Moore, J.G., Fornari, D.J., Clague, D.A., 1985. Basalts from the 1877 submarine eruption of Mauna Loa, Hawaii; new data on the variation of palagonitization rate with temperature. U.S. Geol. Surv. Bull. 1663.
Nayudu, Y.R., 1964. Palagonite tuffs (hyaloclastites) and the products of post-eruptive processes. Bull. Volcanol. 27, 391–410.
Parruzot, B., Jollivet, P., Rébiscoul, D., Gin, S., 2015. Long-term alteration of basaltic glass: mechanisms and rates. Geochim. Cosmochim. Acta 154, 28–48.
Pauly, B.D., Schiffman, P., Zierenberg, R.A., Clague, D.A., 2011. Environmental and chemical controls on palagonitization. Geochemistry, Geophys. Geosystems 12.
Peacock, M.A., 1926. The petrology of Iceland, part 1, the basic tuffs. Trans. R. Soc. Edinburgh 55, 53–76.
Pedersen, L.E.R., McLoughlin, N., Vullum, P.E., Thorseth, I.H., 2015. Abiotic and candidate biotic micro-alteration textures in subseafloor basaltic glass: a high-resolution in-situ textural and geochemical investigation. Chem. Geol. 410, 124–137.
Reyes, A.G., 2000. Petrology and Mineral Alteration in Hydrothermal Systems: From Diagenesis to Volcanic Catastrophes. United Nations University, Geothermal Training Programme.
Romagnoli, C., Jakobsson, S.P., 2015. Post-eruptive morphological evolution of island volcanoes: Surtsey as a modern case study. Geomorphology 250, 384–396.
Schiffman, P., Watters, R.J., Thompson, N., Walton, A.W., 2006. Hyaloclastites and the slope stability of Hawaiian volcanoes: Insights from the Hawaiian Scientific Drilling Project's 3-km drill core. J. Volcanol. Geotherm. Res. 151, 217–228.
Schipper, C.I., Jakobsson, S.P., White, J.D.L., Palin, J.M., Bush-Marcinowski, T., 2015. The Surtsey magma series. Sci. Rep. 5, 11498.
Schipper, C.I., Le Voyer, M., Moussallam, Y., White, J.D.L., Thordarson, T., Kimura, J.I., Chang, Q., 2016. Degassing and magma mixing during the eruption of Surtsey Volcano (Iceland, 1963–1967): the signatures of a dynamic and discrete rift propagation event. Bull. Volcanol. 78, 2–15.
Singer, A., 1974. Mineralogy of palagonitic material from the Golan Heights, Israel. Clay Clay Miner. 22, 231–240.
Singer, A., Banin, A., 1990. Characteristics and mode of palagonite - a review. Sci. Géologiques, Bull. mémoires 88, 173–181.
Spürgin, S., Weisenberger, T.B., Marković, M., 2019. Zeolite-group minerals in phonolite-hosted deposits of the Kaiserstuhl Volcanic Complex, Germany. Am. Mineral. 104, 659–670.
Staudigel, H., Hart, S.R., 1983. Alteration of basaltic glass: mechanisms and significance for the oceanic crust-seawater budget. Geochim. Cosmochim. Acta 47, 337–350.
Staudigel, H., Furnes, H., McLoughlin, N., Banerjee, N.R., Connell, L.B., Templeton, A., 2008. 3.5 billion years of glass bioalteration: volcanic rocks as a basis for microbial life? Earth-Science Rev 89, 156–176.
Stefánsson, V., Axelsson, G., Sigurdsson, O., Gudmundsson, G., Steingrímsson, B., 1985. Thermal condition of Surtsey. J. Geodyn. 4, 91–106.
Stroncik, N.A., Schmincke, H.U., 2001. Evolution of palagonite: crystallization, chemical changes, and element budget. Geochemistry, Geophys. Geosystems 2.
Stroncik, N.A., Schmincke, H.U., 2002. Palagonite - a review. Int. J. Earth Sci. 91, 680–697.
Techer, I., Lancelot, J., Clauer, N., Liotard, J.M., Advocat, T., 2001. Alteration of a basaltic glass in an argillaceous medium: the Salagou dike of the Lodève Permian Basin (France). Analogy with an underground nuclear waste repository. Geochim. Cosmochim. Acta 65, 1071–1086.
Thomassin, J.H., 1984. Étude expérimentale de l'altération des verres silicatés dans l'eau douce et en milieu océanique: apports des méthodes d'analyse de surface des solides (Thèse Doc. ès Sci).
Thorarinsson, S., 1965. Some facts about the Surtsey eruption. Natturufraedingurinn 35, 153.
Thorarinsson, S., Einarsson, T., Sigvaldason, G., Elisson, G., 1964. The submarine eruption off the Vestmann Islands 1963-64. Bull. Volcanol. 27, 435–445.
Thorseth, I.H., Furnes, H., Tumyr, O., 1991. A textural and chemical study of Icelandic palagonite of varied composition and its bearing on the mechanism of the glass-palagonite transformation. Geochim. Cosmochim. Acta 55, 731–749.
Thorseth, I.H., Furnes, H., Heldal, M., 1992. The importance of microbiological activity in the alteration of natural basaltic glass. Geochim. Cosmochim. Acta 56, 845–850.
Türke, A., Nakamura, K., Bach, W., 2015. Palagonitization of basalt glass in the flanks of mid-ocean ridges: implications for the bioenergetics of oceanic intracrustal ecosystems. Astrobiology 15, 793–803.
Von Waltershausen, S., 1845. Ueber die submarinen vulkanischen Ausbrüche in der Tertiär-Formation des Val di Noto im Vergleich mit verwandten Erscheinungen am Aetna. Göttinger Studien.
Walton, A.W., Schiffman, P., 2003. Alteration of hyaloclastites in the HSDP 2 phase 1 Drill Core 1. Description and paragenesis. Geochemistry, Geophys. Geosystems 4.
Walton, A.W., Schiffman, P., Macpherson, G.L., 2005. Alteration of hyaloclastites in the HSDP 2 phase 1 Drill Core: 2. Mass balance of the conversion of sideromelane to palagonite and chabazite. Geochemistry, Geophys. Geosystems 6.
Weisenberger, T.B., Selbekk, R.S., 2009. Multi-stage zeolite facies mineralization in the Hvalfjördur area, Iceland. Int. J. Earth Sci. 98, 985–999.
Weisenberger, T.B., Gudmundsson, M.T., Jackson, M.D., Gorny, C.F., Türke, A., Kleine, B.I., Marshall, B., Jørgensen, S.L., Marteinsson, V.Þ., Stefánsson, A., White, J.D.L., Barich, A., Bergsten, P., Bryce, J., Couper, S., Fahnestock, M.F., Franzson, H., Grimaldi, C., Groh, M., Guðmundsson, Á., Gunnlaugsson, Á.Þ., Hamelin, C., Högnadóttir, Þ., Jónasson, K., Jónsson, S.S., Klonowski, A.M., Kück, J., Magnússon, R.L., Massey, E., McPhie, J., Ólafsson, E.S., Onstad, S.L., Prause, S., Perez, V., Rhodes, J.M., Snorrason, S.P., 2019. Operational Report for the 2017 Surtsey Underwater volcanic System for Thermophiles, Alteration processes and INnovative Concretes (SUSTAIN) drilling project at Surtsey Volcano. ICDP Operational Report. https://doi.org/10.2312/ICDP.5059.001.
Whitney, D.L., Evans, B.W., 2010. Abbreviations for names of rock-forming minerals. Am. Mineral. 95, 185–187.
Zhou, Z., Fyfe, W.S., Tazaki, K., Van der Gaast, S.J., 1992. The structural characteristics of palagonite from DSDP Site 335. Can. Mineral. 30, 75–81.